

APPLICATION OF THE POINT FOCUSING X-RAY MONOCHROMATOR  
TO THE STUDY OF LOW ANGLE DIFFRACTION

Thesis by

Warren Evald Danielson

In Partial Fulfillment of the Requirements  
for the Degree of  
Doctor of Philosophy

California Institute of Technology  
Pasadena, California

1952

## ACKNOWLEDGEMENTS

It is a pleasure to express my sincere appreciation to Professor J. W. M. DuMond for the encouragement and sound advice he has so frequently given throughout the work described below. The lessons in careful experimentation which were learned through association with him are among the most valuable assets of my graduate years.

My sincere thanks are also due Leon Shenfil who shared equally in the design and construction of the point focusing monochromator. He also helped considerably with the earlier latex work, and his analysis of the geometry of the instrument proved very useful in controlling its operation.

Finally I wish to thank my wife, Evalyn, for her confidence and patience throughout these busy years of graduate study.

This project was supported jointly by the Office of Naval Research and the Atomic Energy Commission.

## ABSTRACT

The geometry of the point focusing monochromator is described, and the instrument's uses in connection with low angle diffraction studies are outlined. A careful determination of the particle size of latex spheres by studies of the associated low angle diffraction pattern is made, and an experiment to determine the sensitivity of this particle size to external pressure is described. The results of an experiment in which the monochromator is used to obtain important information on the existence and nature of the collagen molecule are given. A technique for finding the size of particles whose shape is reasonably approximated by two spheroids is given, and the technique is applied to the size determination of bacteriophage type T-4. Improvements in the instrument are discussed and several suggestions for further applications are mentioned.

## TABLE OF CONTENTS

<u>Part</u>	<u>Title</u>	<u>Page</u>
I	THE POINT FOCUSING MONOCHROMATOR . . . . .	1
	Method for Obtaining Focused X Rays . . . . .	1
	Size and Shape of the Focal Spot . . . . .	6
	Position of Scattering Sample and Detector . . . . .	9
	Resolution for Low Angle Scattering . . . . .	10
	Salient Physical Dimensions of the Instrument . . . . .	11
	Means for Detecting Scattered Radiation . . . . .	12
	Use of Helium Gas Along the X-Ray Path . . . . .	13
	Particle Information Most Easily Obtained From Low Angle Diffraction Studies . . . . .	16
II	DETERMINATION OF THE MEAN DIAMETER OF LATEX SPHERES . . . . .	19
	Experimental Data . . . . .	19
	Interpretation of Data . . . . .	30
	Effect of Finite Size of Point Focus . . . . .	36
	Comparison of Samples . . . . .	40
	Use of Relative Intensities at Diffraction Peaks . . . . .	45
	Conclusions . . . . .	46
III	EFFECT OF EXTERNAL PRESSURE ON THE SIZE OF LATEX SPHERES . . . . .	48
	Vacuum-Air Experiment . . . . .	49
	Vacuum-Helium Experiment . . . . .	56
	Conclusions . . . . .	57
IV	INVESTIGATION OF THE LOW ANGLE DIFFRACTION FROM ORIENTED COLLAGEN . . . . .	59
	Sample Preparation . . . . .	60

<u>Part</u>	<u>Title</u>	<u>Page</u>
	Diffraction Pattern Obtained and its Interpretation . .	61
	Conclusions . . . . .	69
V	SCATTERING FROM IDENTICAL NONSPHERICAL PARTICLES RANDOMLY ORIENTED, WITH APPLICATION TO BACTERIOPHAGE T-4 . . . . .	71
	X-Ray Diffraction Pattern from Two Spheroids . . . . .	71
	Application to Particle Size Determination of Type T-4 Bacteriophage . . . . .	76
	Experimentally Obtained Diffraction Pattern of Bacteriophage T-4 . . . . .	80
VI	IMPROVEMENTS IN THE POINT FOCUSING MONOCHROMATOR AND PROPOSALS FOR FURTHER APPLICATIONS . . . . .	84
	Intensity Improvements . . . . .	84
	Miscellaneous Improvements . . . . .	90
	Proposals for Further Applications . . . . .	93
	References . . . . .	95

Part I

THE POINT FOCUSING MONOCHROMATOR

The basic tool used in the studies to be described is the point focusing monochromator, an instrument which was designed and built in Norman Bridge Laboratory. This instrument makes use of a method first proposed by J. W. M. DuMond<sup>(1)</sup> whereby X rays may be brought anastigmatically to a point focus through the use of two elastically bent crystal laminae. Since efficient operation of the instrument requires a knowledge of the way in which the converging monochromatic radiation is obtained as well as a knowledge of the limitations placed on the instrument by its physical construction, it is appropriate that its geometry and design be considered at the outset. A fuller description than the one given below can be found in the doctoral thesis of Leon Shenfil.<sup>(2)</sup>

Method for Obtaining Focused X Rays

The so-called "Bragg" reflection of X rays from crystals following the well known relation

$$n \lambda = 2d \sin \theta$$

produces a reflected beam that is highly selective as regards the wavelength reflected, but one that nevertheless retains, over a very narrow angular domain, almost the full intensity of that particular wavelength in the incident radiation that is in resonance with the crystal lattice. One would therefore expect such reflection to be of prime importance in devising any system for focusing and monochromatizing an X-ray beam. It is well known<sup>(3)</sup> that a particular wavelength of the radiation from a point source may be brought to a line focus by use of a cylindrically

bent crystal as shown in Fig. 1. The three requirements (1) that the angle of incidence of the X rays with the crystal planes used be equal to the angle of reflection, as required by the Bragg law, (2) that this angle be the same for all rays striking the crystal, as required for monochromatization, and (3) that the rays converge to a line focus are seen to be satisfied by a system in which source and focus lie on a circle (the focal circle) defining the concave face of a cylindrically bent crystal, the crystal reflecting "planes" being concentric circular cylinders. The common axis of these cylinders is a line perpendicular to the plane of the focal circle passing through a point,  $\beta$ , on that circle midway between source and focus. Using the fact that an angle inscribed in a circle is equal in radians to half of the intercepted arc, the proof of the above statements is obvious. It is also easy to show that the virtual source for the radiation reflected at P is the point V on the circle through the source S with  $\beta'$  as center.

Since any portion of the crystal lamina shown in Fig. 1 causes those rays which strike it at the appropriate angle to converge as outlined above, one can construct a line focusing monochromator, if desired, by using just a portion of the crystal entirely to the left of the plane of symmetry,  $\beta\beta'$ . For rays in the focal plane, the only difference between the arrangement just suggested and the same arrangement with source and focal point interchanged is that in the latter case the source-to-crystal distance is greater than the crystal-to-focus distance instead of vice versa. Now suppose this latter (second) system is placed so that its focal circle is in a plane normal to that of the first system and so that its crystal intercepts the once reflected beam from the first crystal

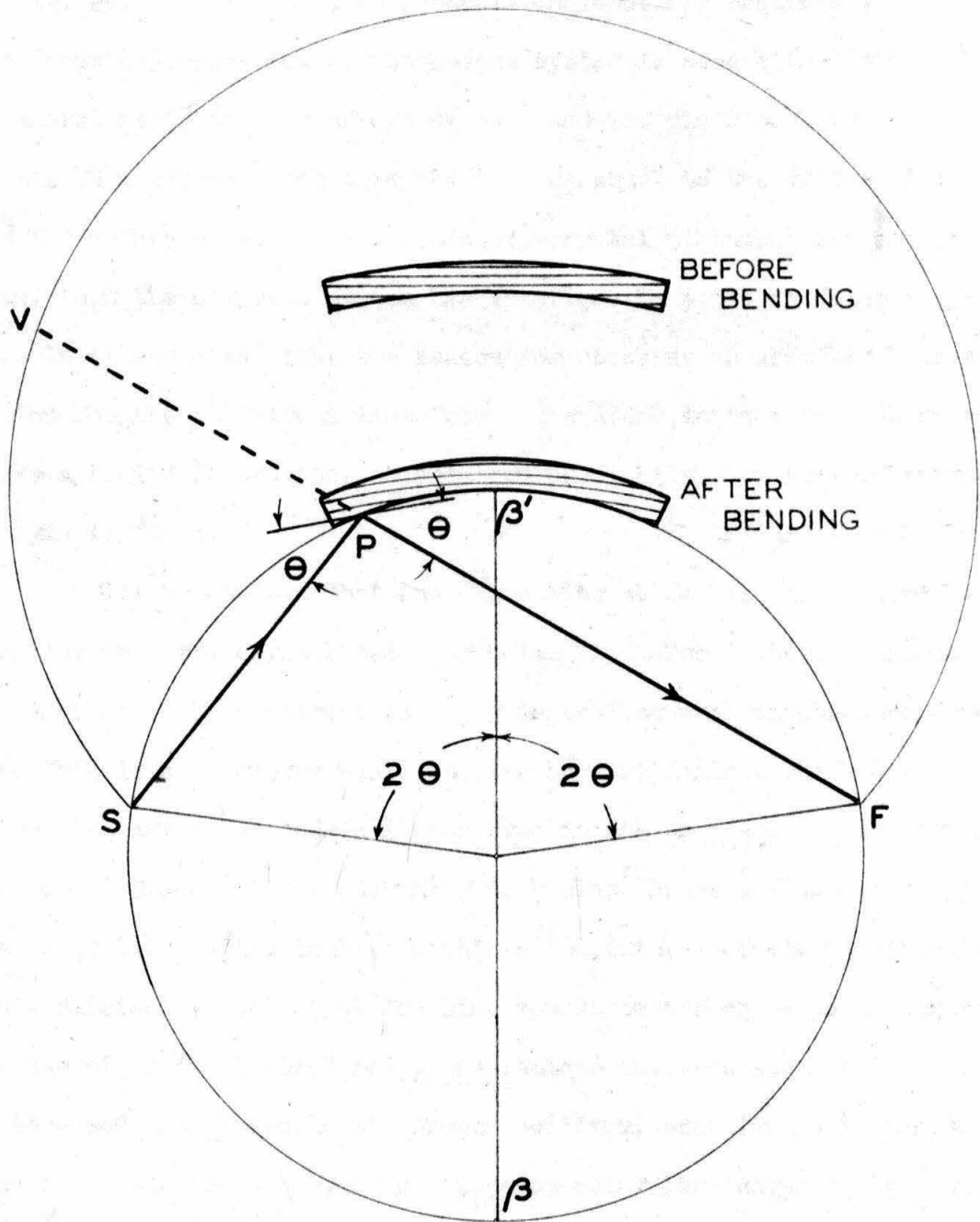


Fig. 1 Showing the focusing action of a single bent crystal lamina, cylindrically ground before bending. (V is the virtual source for radiation from S reflected by the crystal planes at P.)

(see Fig. 2). If, further, the central incident ray required for normal (line focusing) operation of the second system is made coincident with the central reflected ray of system one, and the distance between the crystals as measured along this ray is made equal to the difference between the crystal-to-focus and source-to-crystal distances for either system, then the compound system has anastigmatic point focusing properties. It is now clear that the reason for choosing an asymmetric crystal position for the individual line focusing systems is to allow the crystals to have a finite separation, as required physically, but still obtain an anastigmatic focus.

It will be noticed that the discussion so far is based on the assumption that the crystal faces coincide with arcs of their respective focal circles. The construction of an instrument with crystals conforming to this ideal geometry would require crystal laminae which were ground or otherwise cut to cylindrical arcs even in the unstressed state. This would comprise a difficult machining task since these surfaces would have to be accurately cylindrical to within a few fringes of light. Because of this difficulty, the point focusing monochromator as actually constructed makes use of crystals which are plane laminae in the unstressed state. When stressed and placed in its proper position, each lamina is tangent to the focal circle (the point of tangency being the center of the concave crystal surface), but the surface of the lamina does not coincide with the focal circle over a finite arc, its radius instead being equal to the diameter of the focal circle. Of course the crystal planes are not parallel to the face of the unstressed lamina, but make a constant dihedral angle equal to half the angle measured along the focal circle from  $\beta'$  to

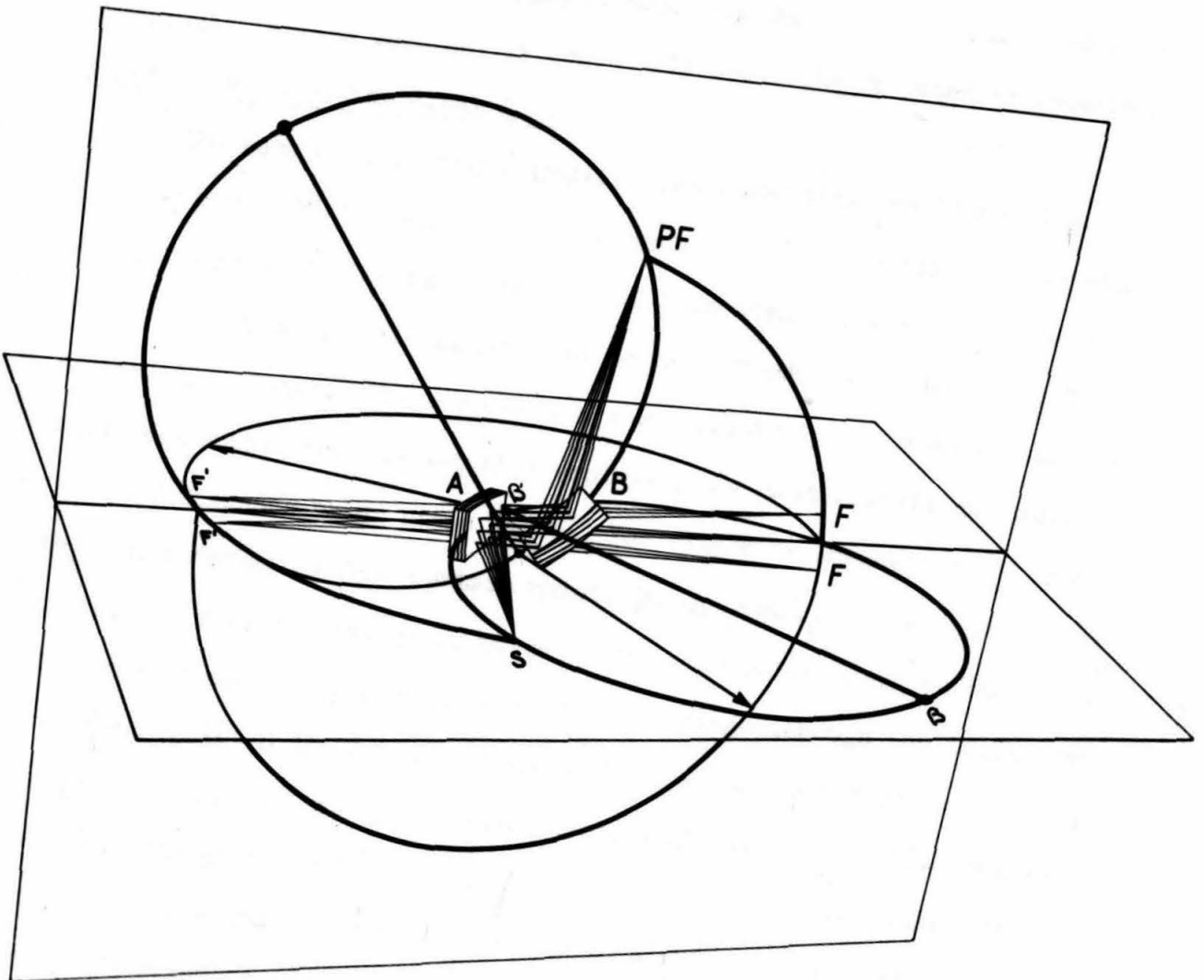


Fig. 2 Showing the 3-dimensional geometry of the point focusing monochromator.

the crystal center with the face of this lamina. This condition makes the crystal planes very nearly concentric about the  $\beta$  point as required.

#### Size and Shape of the Focal Spot

The task of predicting quantitatively the size and shape of the focus obtained with a point focusing instrument of this type was accomplished by L. Shenfil.<sup>(2)</sup> The major results of this analysis will be given here since they give valuable information on the optimum operating conditions for the instrument. These results are qualitatively the same for the ideal system and the one actually employed, the most significant quantitative difference being given below. For either arrangement it is found that only radiation from certain points in an ideally placed broad X-ray source can pass the system by means of two successive Bragg reflections. The projection of these useable points on a plane through the ideal source position (point S in Fig. 1) normal to the central beam turns out to be, in fact, a diagonal strip inclined at about  $45^\circ$  with the horizontal focal circle. The width of this strip depends only on (1) the physical dimensions of those parts of the crystal laminae which receive X-radiation and on (2) whether or not the ideal system (wherein the crystals are ground prior to bending) is used. Using the physical dimensions of the present monochromator, the expected width of this useable strip is 0.2 mm (in excellent agreement with experiment), while the expected width for the ideal case of crystals ground initially to a curve in the unstressed state is 0.1 mm.

For an analytic demonstration that the useable portion of the target is a diagonal strip as mentioned above, reference should be made to Shenfil's thesis. However, qualitative arguments made with reference

to Fig. 2 will demonstrate the existence of such a strip and accurately give its orientation as well:

Consider a point source,  $S$ , (not shown in Fig. 2), situated on a generator of the first focal cylinder (but not necessarily in the horizontal plane containing  $S$  and the centers of the two crystals), this generator being displaced clockwise from the generator through  $S$ . Now just as  $F'F'$  (an arc of the horizontal circle about  $\beta'$  through  $S$ ) is the virtual source for the once reflected beam whose true source is  $S$ , so the corresponding arc,  $F'_1 F'_1$ , of the horizontal circle passing through  $S_1$  with center on a vertical line through  $\beta'$  is the virtual source for the once reflected beam whose true source is  $S_1$ . Furthermore, the wavelength which crystal A can reflect by the Bragg law is proportional to  $\sin \theta$  (see Bragg equation, p. 1), hence the wavelength to be ascribed to any such virtual source depends only on the angular position (along the focal circle) of the true source from the crystal. Hence, since  $S_1$  was assumed to be displaced in a clockwise direction from  $S$ , the wavelength associated with arc  $F'_1 F'_1$  and its radius of curvature are less than the corresponding wavelength and radius of curvature, respectively, of  $F'F'$ .

Now in order for radiation from arc  $F'_1 F'_1$  to be efficiently reflected by crystal B,  $F'_1 F'_1$  must intersect the vertical focal circle at a point,  $Q$ , so situated that the angle with which rays from this point strike crystal B is equal to the Bragg angle for that particular wavelength associated with  $F'_1 F'_1$ . Since a given displacement from  $F'F'$  along the vertical focal circle corresponds to the same wavelength change (in the radiation reflected by crystal B) that occurs (in the radiation reflected by crystal A) for an equal displacement along the horizontal focal circle from  $S$ ,

this last requirement can be met only if  $S_1$  is as far below the plane of the horizontal focal circle,  $\beta S \beta'$ , as is point Q.

Designating the angular arc from  $\beta'$  to A (i.e., the center of crystal A) by  $2\alpha$ , it follows that the projection of points satisfying this last requirement on a plane through S normal to SA is a line through S whose angle with the horizontal is  $\tan^{-1} \frac{\sin(\theta + \alpha)}{\sin(\theta - \alpha)}$ . Thus for  $\alpha$  small in comparison to  $\theta$ , this angle is very nearly  $45^\circ$ , its value for the present instrument ( $\theta = 40.7^\circ$ ,  $\alpha = 2.1^\circ$ ) being  $47.3^\circ$ .

By virtue of the symmetry of the entire system with respect to an interchange between "point" focus and X ray source, it follows that this focus (i.e., the locus of the points in which the converging beam intersects a plane through PF normal to the central ray of this beam) is also essentially a line inclined at  $47.3^\circ$  with respect to the vertical focal plane. The breadth of this "line" is determined by the solid angle subtended about the X-ray source by the crystal lamina and is about 0.2 mm for the instrument under discussion. Since there is a wavelength difference between the radiation focused at one point along this strip and that focused at another, the crystal laminae can be so adjusted that the wavelength of the radiation focused at the center of this strip is the same as that of a strong X-ray line in the characteristic spectrum of the target material of the X-ray tube used as source. The "length" of the focal strip will then be limited by the natural breadth of this line. Using the  $K\alpha_1$  line of the copper target presently being used, the "length" of this focal strip is about 1.4 mm.

Having established the close correspondence between the focal strip and the useable projected target area, it becomes clear that the energy

in the monochromatic, converging beam is proportional to the energy passing through the useable target strip in the direction SA. Borrowing terms from the field of optics, this result can be restated: The energy in the converging beam is proportional to the luminance of the X-ray source as viewed along AS, provided the source fills the useable target window.

Before applying the foregoing results to a discussion of the resolution control possible with the instrument, some information about the position of the sample to be studied and the type of data obtained is in order.

#### Position of Scattering Sample and Detector

In view of the fact that information concerning the particle size and/or shape is to be obtained from a study of the X-rays scattered through small angles (in a range from about 0.002 to 0.1 radians), it is very important that the detection of the scattered radiation be made where the position of detection (in the case of a true point focus) uniquely determines the scattering angle. This is possible only if detection is made in the focal plane (i.e., the plane through PF normal to the converging pencil of rays). Consequently the sample must be placed in the converging monochromatic beam between crystal B and the point focus, PF. If all parts of the scattering sample are equally distant from PF, then all rays scattered by the sample through a given (small) angle will be detected at essentially the same lateral distance from the point focus.

A very high percentage of the fairly long X-radiation (say  $\lambda > 1\text{\AA}$ ) scattered at small angles by particles with characteristic diameters of from a few angstroms to a few thousand angstroms is scattered coherently.

In such cases the total diminution of the X-ray intensity in traversing a single particle is so small that it can be neglected. The small angle intensity pattern produced by such particles is in good agreement with the classical assumptions (1) that the electrons of the scattering particle are forced to vibrate with the frequency of the field vectors which describe the X-ray beam and (2) that these electrons must therefore radiate electromagnetic energy of this same frequency. This ideal low angle scattering of X rays by particles in the size range under consideration is thus a volume effect -- all of the electrons in the particle contribute to the scattered radiation.

#### Resolution for Low Angle Scattering

Using this theory, it is easy to show that in the case of X-ray diffraction, as in the case of the diffraction of optical light (although diffraction in this case is more of a surface effect), the pattern obtained from a series of randomly placed but similarly oriented identical particles is the same as the pattern due to a single particle. In such cases the intensity pattern produced by a truly point focusing beam will have regions where the intensity is a relative maximum and others where it is a relative minimum, the separation of successive extrema being of the order of  $\frac{\lambda}{D}$  radians where  $\lambda$  is the wavelength of the radiation used, and  $D$  represents the average particle diameter. If, now, the direct beam is finite, but small in comparison with the distance between adjacent extrema, the detail of the pattern can still be observed. In keeping with this qualitative idea of "resolution" as the ability to see detail, the resolution obtainable with a monochromatic X-ray beam is defined as  $\frac{\lambda d}{2w}$  and is measured in  $\text{\AA}$ . (Here  $d$  is the sample-to-detector distance, and  $w$  is the beam diameter at the detector.) The resolution in  $\text{\AA}$  thus designates

the approximate size of the scattering particle whose relative intensity extrema can just be clearly observed. It should be noted that resolution is thus a function of the sample position, and that the study of large particles requires correspondingly high resolution.

When equal resolution is desired in all directions in the focal plane, the "point" focus must obviously be as nearly circular as possible. This means that the length and width of the focal strip described above ( p.8 ) should be equal. As mentioned above, the width depends on the solid angle of radiation being used by the crystals, and hence can be controlled by "stopping down" the crystals. This width is, however, several times smaller than the length of the strip, and no practical advantage in utilizing this control, for the samples so far studied, has been found. Since the length of the focal strip cannot be greater than that of the useable target strip, this length can be controlled by placing a suitable slit in front of the X-ray tube. A judicious choice of these parameters (the length and width of the focal spot) allows one to obtain the necessary resolution for a given experiment while keeping the total intensity as high as the required resolution will permit.

#### Salient Physical Dimensions of the Instrument

Since the alignment procedure for establishing the proper orientation between the X-ray source and the two elastically bent crystal laminae, while exceedingly important in obtaining the point focus itself, does not enter into procedures followed in actually using the instrument, it will suffice to state that a careful, systematic method of alignment has been worked out and is described in reference (2). Certain physical dimensions of the instrument are, however, essential to an appreciation of both its capabilities and its limitations.

The radius of the focal circles is nominally 60 cm, and the angular displacement of the crystals along the focal circle from the  $\beta'$  point is about  $4^\circ$ . The crystal planes utilized in producing the Bragg focusing are the 310 planes of quartz, and the radiation which is focused by the instrument is the  $\text{Cu K}\alpha_1$  line ( $\lambda = 1.5374$ ), hence the Bragg angle is approximately  $40.7^\circ$ . These quantities, together with the finite size of the crystal laminae and their clamping blocks, determine the maximum specimen-to-film distance that can be obtained, this distance being about 65 cm. The dimensions of the crystal laminae are such that the cross-section of the X-ray beam midway between the crystals is approximately a square 2 cm on a side. Under normal operating conditions, no "stop" is provided in front of the X-ray tube so that the focal spot is an elongated region with major and minor diameters of about 1.7 mm and 0.2 mm respectively.\* Thus, for applications in which the scattered radiation to be studied shows a particular directional orientation, one can obtain the maximum amount of scattered intensity with very little loss in resolution by orienting the sample so that the preferred scattering direction is along the minor axis of the focal spot.

#### Means for Detecting Scattered Radiation

As already suggested, the amount of radiation that goes into low angle scattering is in most cases extremely small. For this reason, X-ray film (Eastman medical duplitized, no-screen) has been principally used, the use of Geiger counters being limited to measurements of the direct beam intensity. Film techniques have other advantages over counters for the study of the low angle diffraction from substances which give rather

---

\* See p. 8

complicated patterns in that a single film provides the complete record of such a pattern whereas a two dimensional scanning of the entire focal plane by a counter with a very small window would be required to obtain the same information. It must be admitted, however, that for absolute intensity comparisons a counter method far excels one utilizing film.

#### Use of Helium Gas Along the X-Ray Path

Provision has been made for the X rays, after passing through the window of the X-ray tube, to spend the remainder of their traversal of the point focusing monochromator in an atmosphere of helium. The most important reasons for choosing helium as the medium through which the X rays are propagated are threefold: (1) The attenuation of the beam in helium gas is very slight -- a medium of helium at a pressure of one atmosphere causes only a 2% attenuation of the beam in traversing the 160 cm path of the point focusing monochromator. Thus the low absorption advantage of a vacuum system is obtained without the construction and operational difficulties of such a system. (The quantitative advantages of a helium system over an air-filled system are given in the section on intensity improvements in Part VI.) (2) Scattering (as distinguished from total absorption) of Cu  $K\alpha$  radiation by a helium atom is very much less than by an oxygen or nitrogen molecule, so that by using helium one obtains a second major advantage which a vacuum system has over a medium of air without the accompanying inconveniences. (3) With the helium system, wet samples can be conveniently introduced into the beam merely by enclosing them in a thin sheet of nylon (for which absorption is extremely low), the moisture being maintained by a vapor-tight beeswax seal at points outside the path of the scattering beam. Such samples could be used only with

difficulty in a vacuum system. The great advantage in being able to use wet samples lies in the fact that many of the substances whose particle sizes or periodicities are such as to be amenable to study by the point focusing monochromator are biological in nature, with properties that are greatly altered by desiccation. Thus the physical disposition of the atomic constituents making up the substance may also undergo considerable change in drying, the phenomenon of shrinkage being the most obvious one. Hence, measurements made on the substance in its natural environment would be a valuable supplement to measurements of the substance after desiccation. In part of the size range (from say 20 to 3000 Å) where low angle diffraction studied with the present instrument are useful, the electron microscope provides a very powerful tool for ascertaining size and structure; however, the limitation to samples which are desiccated is especially severe for this instrument.

Fig. 3 shows the instrument in its present form. The box-like enclosure into which the (horizontal) metallic tube leading from the X-ray source projects contains the two crystal clamping blocks with their respective crystal laminae. This box-like enclosure, the horizontal tube, and the rectangular nearly vertical column provide the envelope containing the helium as well as acting as radiation shields and light shields. Moreover, the vertical column is provided with a series of shelf-like openings into which a sample holder can be inserted, much as a drawer, and cover plates with O-ring seals can be securely fastened over them to render the system helium-tight. These "shelves" were carefully machined and their separations accurately measured so that, in the case of samples whose effective distance from the point focus could not be

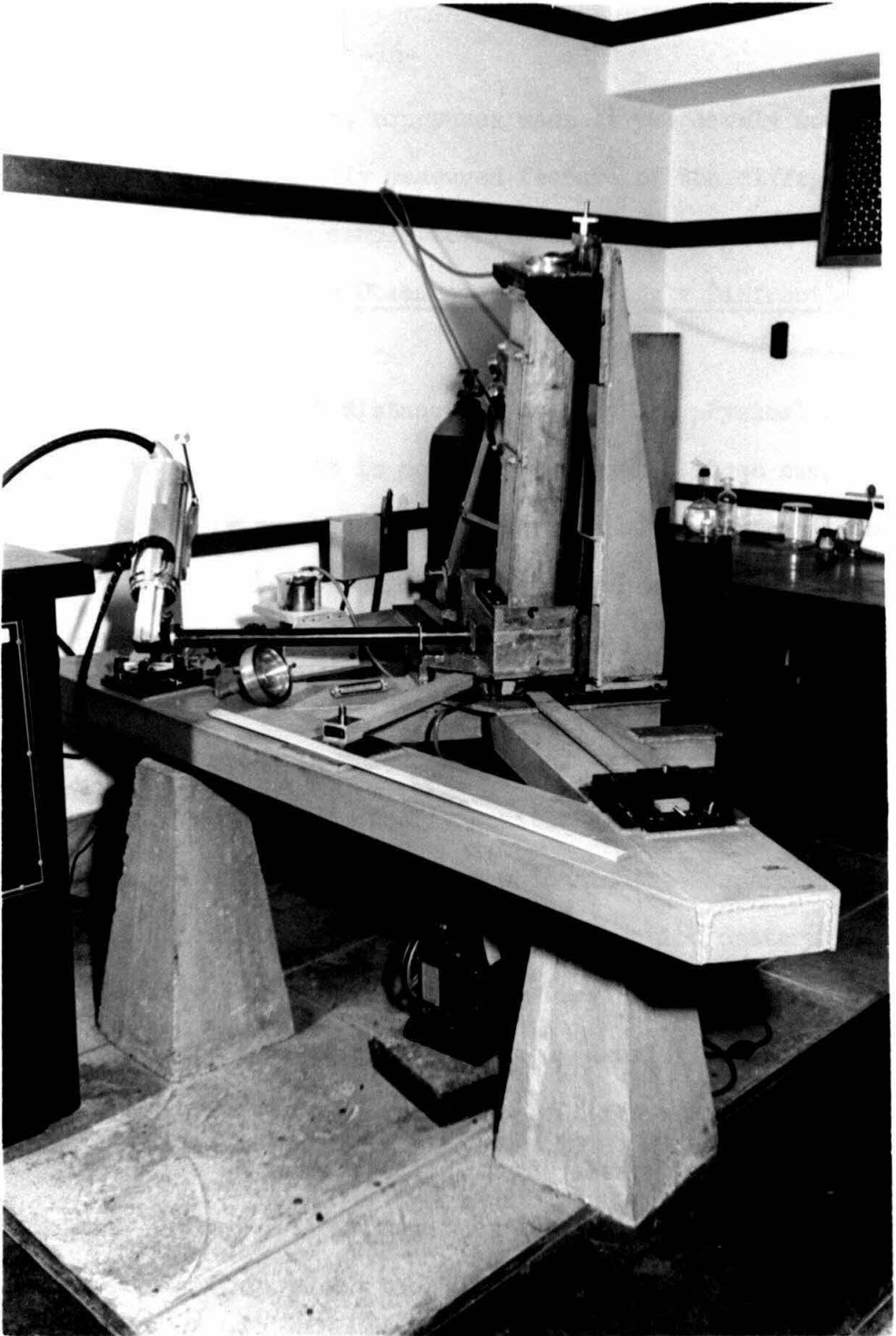


Fig. 3 The complete instrument.

directly measured with precision, exposures made at two levels would, by triangulation using some easily measured feature of the diffraction pattern, furnish the effective sample-to-film distance for both exposures.

Particle Information Most Easily Obtained From Low Angle Diffraction Studies

In view of the fact that distance is usually the physical quantity most amenable to measurement, it is not surprising that those sample features which are simply related to the positions of the intensity maxima and minima in the diffraction pattern are the features concerning which quantitative information can be most easily obtained. Two examples of samples with features of this type which have been measured with the present instrument can be cited in this connection. First, a substance made up of many equal spheres with no orderly positional arrangement among the spheres will produce a diffraction pattern which is the superposition of the intensities of all the spheres, hence the diffraction pattern is the same for the collection of spheres as for any single one of them. Since the pattern for a single sphere with an electron density that depends only on the radial distance from the center shows relative maxima and minima that depend only on the scattering angle, it is clear that the pattern obtained from such a sample with a point focusing instrument will possess a series of concentric rings along each of which the intensity is a maximum or minimum. Consequently, an accurate measurement of the sphere size can be obtained from a measurement of the ring sizes, the task being even easier when the radial electron density is known. Second, the constituent parts of a substance may possess a one dimensional periodicity and be oriented in the same direction. Under such conditions the pattern obtained will possess

a directly related period, so that again the sample period can be found by making distance measurements.

In addition to furnishing a record from which positions of intensity maxima and minima can be found, the film exposed by the diffracted X rays also furnishes a complete record of the way in which the intensity varies from point to point. Now the intensity scattered in a given direction is, for the wavelength employed, uniquely determined by the projection of the electron density of the sample onto a plane normal to the bisector of the scattering angle. Hence low angle diffraction studies essentially depend only on the projection of the electron density onto a plane normal to the central beam. It is thus clear that low angle X-ray diffraction data cannot, even theoretically, completely determine the electron distribution in the sample, but only the projection of this distribution. Consequently, particle shape and size distribution cannot be simultaneously inferred; however, if the shape is known, the distribution of sizes in the sample can often be approximately found and vice versa. For such determinations it is almost always essential that the relative X-ray intensities be known over a finite range of the diffraction pattern (instead of knowing only the positions of relative intensity extrema).

When the particles are known to have a particular shape (say from electron microscope pictures), the approximate size distribution is most easily found by comparing the obtained intensity pattern with a theoretical pattern containing appropriate parameters to describe the types of size distribution most likely to occur in nature (e.g., Gaussian, Maxwellian, and rectangular). By comparing the experimental intensity pattern with families of theoretical patterns such as those just suggested, one

can obtain the size distribution to a fair degree of accuracy. If the particles are randomly oriented spheroids (including spheres and long cylinders as special cases), the task of composing many theoretical comparison patterns has already been carried out by Roess and Shull<sup>(4)</sup>, their results being given in the Journal of Applied Physics (1947) 18, 295. An example in which the present instrument has been used for a sample of this type (carbon black) is given in L. Shenfil's thesis.<sup>(2)</sup> The more complicated problem of treating a particle made up of two connected spheroids is discussed in Part V.

Part II

DETERMINATION OF THE MEAN DIAMETER OF LATEX SPHERES

A determination of the mean particle size of latex spheres by observing the X-ray diffraction pattern obtained with these objects as scatterer was first carried out by Yudowitch<sup>(5)</sup> using slit-system collimation and approximate monochromatization by filtration. Widespread interest<sup>(6)</sup> has been shown in the particle size of the now famous Dow latex, batch 580-G, lot 3584, extensively used as a valuable comparison standard of size for electron microscopes (which have revealed that they consist of spherical particles about 2600 Å units in diameter). This widespread interest, coupled with the belief that the precision with which this size can be obtained from X-ray diffraction data could be increased, have provided the impetus for the latex diffraction studies to be described. The basic approach to the problem is similar to that taken by Yudowitch, but advantage has been taken of the highly monochromatic sharply converging beam afforded by the point focusing monochromator.

Experimental Data

The samples of latex used were taken from 5 cc vials containing 40% water suspension of latex\* (these are the standard containers and contents sent to electron microscopists by the Dow Chemical Company). The water was removed by evaporation, and about 0.4 cc of the latex powder was placed between 1 mil nylon sheets in a cavity of dimensions 2 x 2 x 0.1 cm. This

---

\* One of these samples was kindly loaned to us by Dr. R. F. Baker of the University of Southern California, the other was obtained later through the much appreciated cooperation of Dr. K.L. Yudowitch.

sample was then placed in the converging beam slightly above the second crystal of the point focusing monochromator with the 2 x 2 cm square faces normal to the central ray which passes through the centers of the squares. The sample-to-film distance is given below in conjunction with the other quantitative experimental data (the film is, of course, normal to the central ray at the point focus with its center coinciding with the point focus). The observed diffraction pattern consists of a series of well defined rings corresponding to intensity maxima for various (small) angles of deviation in the X-ray beam.

Fig. 4 shows typical diffraction patterns obtained with "coarse" and "fine" adjustment of the focus respectively. In the "coarse" adjustment, the length of the slightly elongated focus is sufficient to blur out the successive diffraction rings in one azimuth as can be clearly seen, while in the "fine" adjustment the "point" focus is sufficiently short along its greatest dimension to make the rings distinguishable in all azimuths. The dark portion in the center of the left hand picture is a hole in the film to permit the direct beam to pass freely through the film without undue fogging. Successive rings, which are seen to be clearly resolved, are separated by a difference of scattering angle of about 0.002 radians. Fig. 5 shows a microphotometer trace of the 129.4 hour exposure made using high resolution.

In compiling the data, use has been made of diffraction photographs taken with three physically distinct samples of the Dow latex particles. Two of these, designated as samples I-a and I-b, respectively, were from physically distinct portions of the latex loaned to us by Dr. Baker of U.S.C., and the third sample, designated as sample II, was latex from the

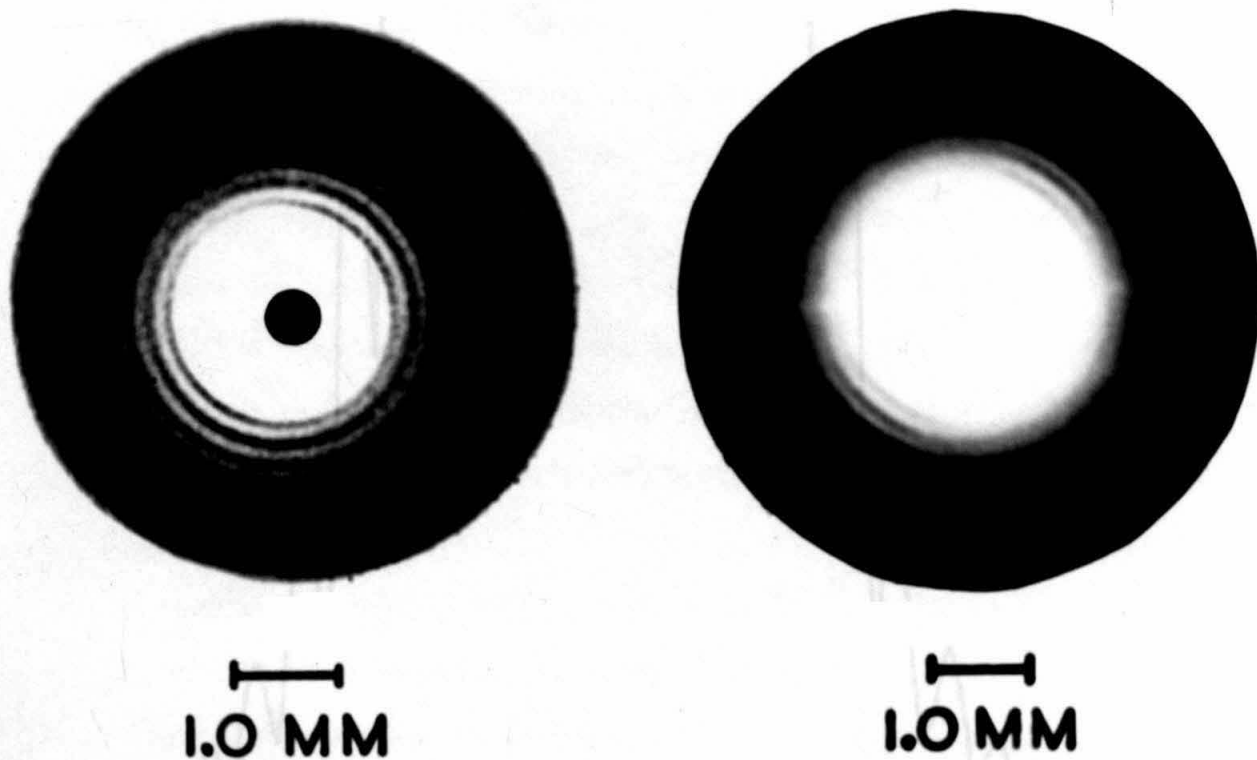


Fig. 4 The diffraction pattern reproduced on the left was obtained in 129.6 hours using sample I-b with the "fine" focus arrangement, while the one on the right was obtained in 91.1 hours using sample II with full intensity.

Fig. 5 Inter curve of diffracting patterns of same particles sample I-b, fine focus, 4.5 x 4 hr. intervals as the bottom reversed 0.50 sec on the diffracting pattern at a scattering angle of about 3 minutes of arc.

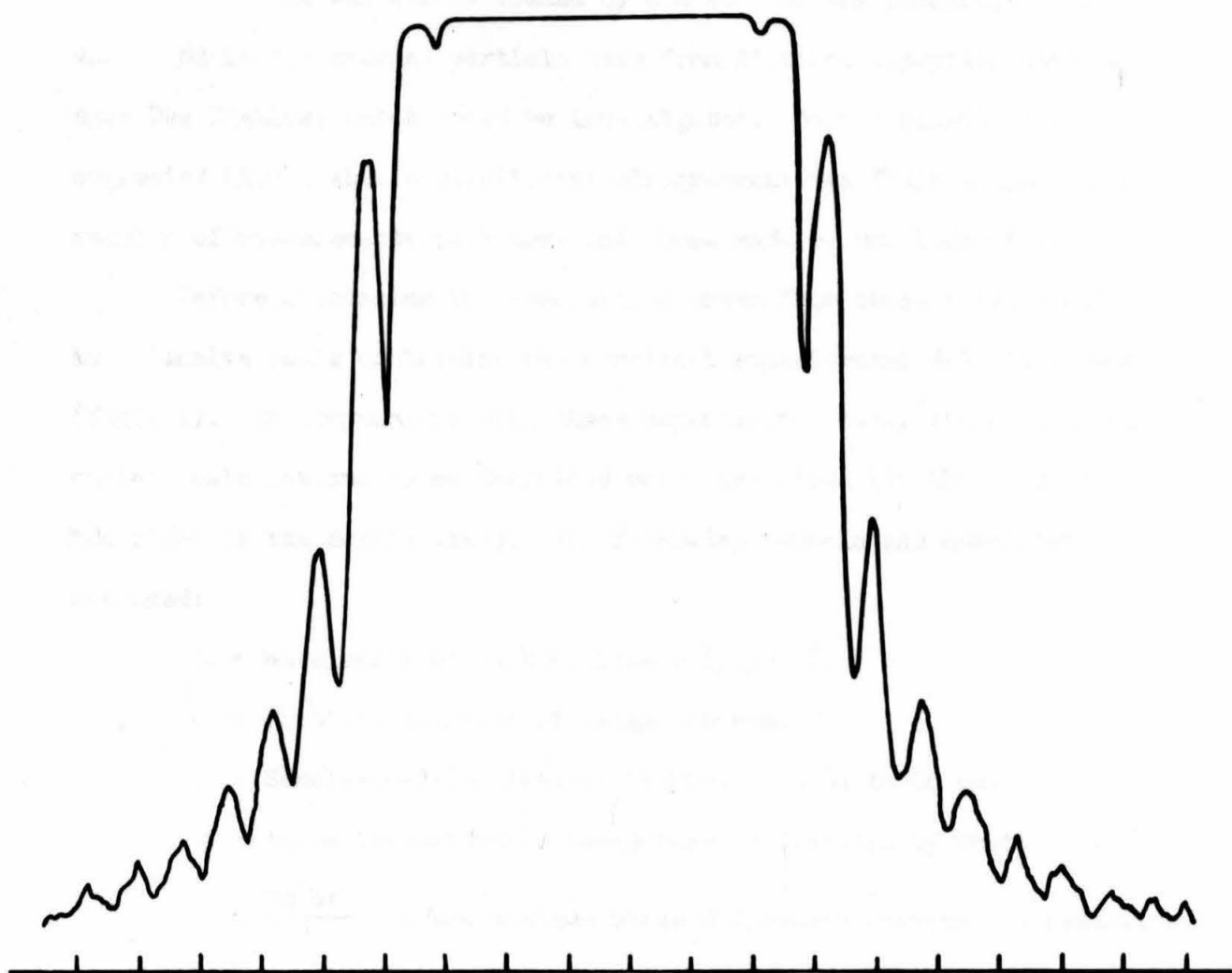


Fig. 5 Microphotometer curve of diffraction pattern of latex particles (sample I-b, fine focus, 129.4 hr. exposure). Intervals at the bottom represent 0.50 mm on the diffraction pattern or a scattering angle of about 3 minutes of arc.

same 5 cc vial as that used by K. L. Yudowitch<sup>(5)</sup> in his work on latex. This last sample was kindly loaned by him so that the possibility of variation in the average particle size from distinct apportionments of the same Dow Chemical batch could be investigated. Such a possibility suggested itself when a significant disagreement was found between the results of measurements made here and those made by Dr. Yudowitch.

Before discussing the conclusions drawn from these measurements, an extensive table containing the pertinent experimental data is presented (Table I). In conjunction with these experimental data, the results of certain calculations to be described below are given (in the columns to the right of the double line). The following symbols and numerical values are used:

$\lambda$  = Wavelength of Cu  $K\alpha_1$  line = 1.5374 Å.

D = Particle diameter of latex spheres.

d = Sample-to-film distance (varied from 64 to 66 cm)

$\epsilon$  = Angle through which x-ray beam is deviated by scatterer.

$u = \frac{2\pi D\epsilon}{\lambda}$  is the maximum phase difference between the radiation scattered in a direction  $\epsilon$  by an element at the center of the sphere and that scattered in the same direction by any other element. (See Fig. 6).

$\Delta$  = Estimated accuracy limit in measuring a diffraction ring radius. It is believed that this estimation is such that about 90% of all observations would fall inside the range  $\pm \Delta$ .

w = Weight to be attached to a given measurement.

Values for successive diffraction ring radii were measured from microphotometer traces such as the one shown in Fig. 5; the microphotom-

Table I

Sample and film description	Peak Number	$(\epsilon d)_{\text{ave}}$ (mm)	$\Delta$ (mm)	w	$D(\text{\AA})$ ( $P=0$ )
I-a 21 hrs. $d = 642.8 \pm .5$ mm	5	1.800	.016	1262	2711.2
	6	2.172	.020	1177	2706.8
	7	2.555	.029	776	2690.5
	8	2.922	.035	687	2692.7
I-a 23.7 hrs. $d = 642.8 \pm .5$ mm	5	1.815	.020	216	2688.9
	6	2.180	.028	1188	2696.8
	7	2.535	.029	819	2711.9
	8	2.870	.035	980	2741.4
	9	3.288	.032	882	2694.9
	10	3.678	.034	1322	2678.5
	11	4.020	.050	1392	2697.4
I-a 80.7 hrs. $d = 642.8 \pm .5$ mm	12	4.375	.039	766	2704.9
	7	2.533	.036	496	2714.1
	8	2.888	.035	681	2724.4
	9	3.305	.021	2475	2681.0
	10	3.658	.022	2766	2688.3
	11	4.033	.030	1803	2688.6
	12*	4.392	.029	2280	2691.5*
	13*	4.754	.034	1954	2694.6*
14*	5.115	.030	2940	2682.1*	

Table I (continued)

Sample and film description	Peak Number	$(\epsilon d)_{ave}$ (mm)	$\Delta$ (mm)	w	$D(\overset{\circ}{\text{A}})$ ( $P=0$ )
	15*	5.511	.041	1890	2687.9*
	16*	5.865	.065	835	2689.8*
I-a 5 hrs. d = 642.8 $\pm$ .5 mm	5	1.798	.024	561	2714.4
	6	2.162	.028	596	2719.1
	7	2.532	.029	762	2715.0
	8	2.885	.044	429	2727.6
	9	3.280	.069	226	2701.5
I-a 41.6 hrs. d = 642.8 $\pm$ .5 mm	6	2.185	.040	298	2690.5
	7	2.548	.040	406	2698.8
	8	2.900	.032	821	2713.1
	9	3.292	.024	1882	2691.4
	10	3.655	.035	1088	2695.5
	11	4.035	.028	2076	2687.3
	12*	4.398	.024	3360	2687.9*
	13*	4.775	.036	1760	2683.1*
	14*	5.130	.042	1492	2690.1*
	15*	5.508	.045	1500	2684.9*
	16*	5.900	.060	968	2674.0*
	17*	6.240	.075	693	2686.8*
I-b 4.5 hrs. d = 661.97 $\pm$ .35 mm	5	1.880	.060	87	2673.5

Table I (continued)

Sample and film description	Peak Number	$(\epsilon d)_{ave}$ (mm)	$\Delta$ (mm)	w	D( $\text{\AA}$ ) (P = 0)
I-b 129.4 hrs. (narrow focus)  d = 661.97 $\pm$ 0.35 mm	5	1.875	.025	562	2680.7
	6	2.248	.019	1400	2693.3
	7	2.640	.019	1932	2681.6
	8	3.015	.030	1010	2687.4
	9	3.420	.036	902	2668.0
	10	3.758	.039	929	2699.8
I-b 178.95 hrs. (med. focus)  d = 661.97 $\pm$ 0.35 mm	11	4.140	.048	743	2697.2
	6	2.240	.045	248	2702.7
	7	2.640	.028	889	2681.6
	8	3.012	.025	1432	2690.0
	9	3.400	.022	2386	2683.6
	10	3.770	.025	2273	2691.3
	11	4.135	.034	1436	2700.4
12*	4.530	.032	2000	2686.8*	
13*	4.905	.042	1360	2689.6*	
14*	5.300	.062	782	2681.2*	
I-b 18.9 hrs.  d = 661.8 $\pm$ .4 mm	5	1.856	.029	410	2707.2
	6	2.212	.026	724	2736.3
	7	2.625	.029	819	2696.2
	8	2.995	.031	933	2704.9
	9	3.388	.032	1120	2692.6
	10	3.780	.052	528	2683.5

Table I (continued)

Sample and film description	Peak Number	$(\epsilon d)_{ave}$ (mm)	$\Delta$ (mm)	w	D( $\text{\AA}$ ) (P=0)
II 68.2 hrs. d = 661.39 $\pm$ 0.3 mm	5	1.882	.038	245	2668.2
	6	2.242	.021	1145	2698.0
	7	2.635	.026	1027	2684.4
	8	2.972	.030	982	2723.9
	9	3.378	.020	2856	2698.7
	10	3.785	.022	2958	2678.3
	11	4.152	.032	1682	2687.0
	12*	4.505	.055	672	2699.8*
13*	4.868	.058	705	2707.4*	
II 44.3 hrs. d = 661.6 $\pm$ .3 mm	5	1.872	.031	365	2683.0
	6	2.238	.018	1545	2703.7
	7	2.632	.022	1428	2688.2
	8	3.000	.029	1070	2699.5
	9	3.378	.024	1473	2699.5
	10	3.778	.035	1166	2684.0
	11	4.160	.053	616	2682.7
II 5.95 hrs. d = 661.39 $\pm$ .3 mm	5	1.865	.035	284	2692.5
	6	2.238	.028	638	2702.9
	7	2.625	.038	477	2694.5

Table I (continued)

Sample and film description	Peak Number	$(\epsilon d)_{ave}$ (mm)	$\Delta$ (mm)	w	D( $\text{\AA}$ ) (P=0)
II 91.1 hrs. d = 661.80 $\pm$ .3 mm	6	2.240	.042	284	2702.0
	7	2.635	.025	1113	2686.1
	8	2.972	.022	1825	2725.6
	9	3.352	.021	2544	2721.4
	10	3.768	.026	2103	2691.9
	11	4.158	.030	1918	2684.8
	12*	4.505	.035	1658	2701.5
	13*	4.912	.044	1245	2687.3

\* The asterisk indicates measurement from microphotometer trace using wide slit as explained in text.

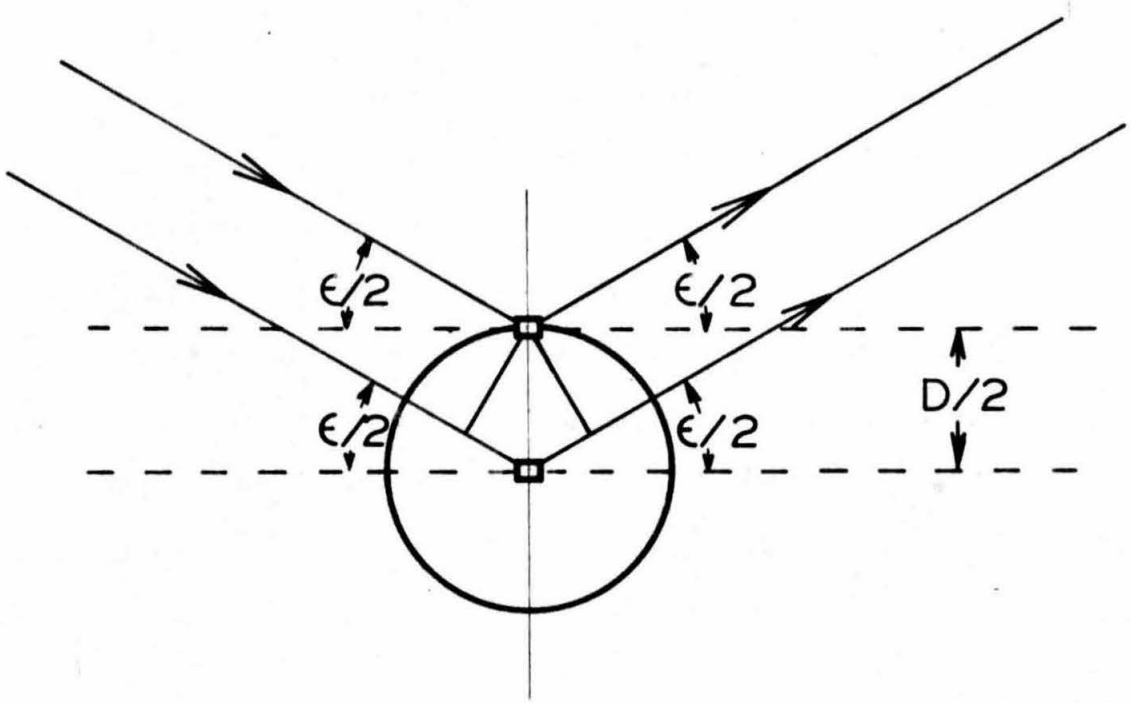


Fig. 6 To illustrate the significance of the phase difference,  $u$ .

eter "window" size for most of the traces corresponds to a film area of 0.06 x 0.13 mm. For the weaker, larger diameter, diffraction rings (rings beyond No. 11), it was found that the effect of film grain could be lessened, and consequently more reliable results obtained, if the "window" were lengthened and an experimental correction made for the systematic error so introduced. Rings so measured and corrected are indicated with an asterisk.

#### Interpretation of Data

In order to be able to infer particle sizes for the latex spheres from the entire series of rings, consideration has been given to at least three possible space arrangements of the particles relative to each other in each of which the particle diameter might be expected to influence the diffraction pattern differently.

(1a) The spheres may tend to clump, in the process of drying, in such a way that the interior of each clump is made up of a close-packed hexagonal or cubic array of particles like a crystallite in a polycrystalline solid, the orientation of the clumps being random.

(1b) It is also conceivable that, since the particles are large enough that the interparticle forces probably do not have the nature or intensity of the interatomic forces in crystals, the spheres may tend to form a close-packed array that is a hybrid of the hexagonal close packing (layer scheme A, B, A, B, A, B etc., see Fig. 7) and the cubic close packing (layer scheme A, B, C, A, B, C etc.) such that the layers in which each sphere makes contact with six others are placed unsystematically upon one another instead of having a definite relation to the lower layers.

(2) The particles surrounding any arbitrarily chosen particle

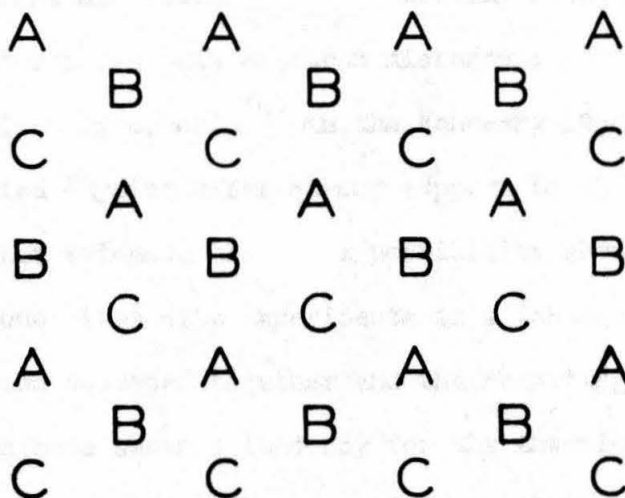


Fig. 7 To illustrate the close-packed arrays considered in the text. Any set of like letters is to be thought of as representing the centers of spheres in a given horizontal plane. The different letters are then to be thought of as lying in different horizontal planes.

may fall into a spherically symmetric arrangement similar to that commonly assumed as representative of the disposition of atoms in a liquid, but with no other more far-reaching type of regularity markedly present.

(3) The particles may be distributed with sufficient lack of regularity that the distribution is essentially random.

One might suppose that electron microscope pictures of the latex such as those given by Gerould<sup>(6)</sup> in the February 1950 issue of the Journal of Applied Physics offer strong support to the first possibility, (1a). (As further evidence that this possibility should receive careful consideration, one might cite experiments in which equal spheres of bread or putty have been squeezed together and the resulting arrangement studied. Such experiments have shown a tendency for the interior particles to form a cubic close-packed array.) However, if crystal-type packing were the major cause for the observed diffraction rings (as in a Debye-Scherrer powder pattern) there would be a series of rings corresponding to each fundamental spacing of "crystallite" planes containing a high surface density of particles. Hence the fact that only a single distinct series of rings is obtained seems to be proof that such scattering is at most a minor contributor to the diffraction pattern. The other possibility, (1b), of a hybrid "crystal" built up as outlined above would indeed lead to clumps with only one fundamental set of interplanar spacings. However, such an interpretation of the results yields a value for the particle size that is wholly incompatible with electron microscope values, and furthermore, the relative intensities between successive rings as observed do not correspond to those which would be expected in such a case.

The development of a rather idealized theory to describe the space

arrangement of the particles as conceived under (2) above was given by Gingrich and Warren<sup>(7)</sup> in 1934, and has been applied to the present problem by K. L. Yudowitch.<sup>(5)</sup> The main simplifying assumption underlying the theory is that the number of spheres per unit volume, as a function of the radial distance ( $r$ ) from an arbitrarily chosen sphere, is essentially constant except for a peak at  $r = D$  and a void for  $r < D$ . To describe the size of the peak at  $r = D$ , a "packing" parameter ( $P$ ) is introduced. It is so defined that  $P=0$  corresponds to a random distribution of spheres, hence case (3) considered above is included in this treatment. Denoting the X-ray intensity scattered at an angle  $\epsilon$  by  $I$  and setting  $M$  = number of spheres in the sample,  $N$  = number of electrons per sphere and  $\Phi(u) = \frac{3}{u^3} (\sin u - u \cos u)$ , the simplification mentioned above leads to the following formula:

$$I = M N^2 \Phi^2(u) \left[ 1 + P \left\{ 5 \frac{\sin 2u}{2u} - 6 \Phi(2u) \right\} \right] \quad (1)$$

$\Phi(u)$  is zero when  $\tan u = u$  (except at  $u=0$ ), hence  $I$  has an oscillatory character that would account for a series of intensity maxima. Insofar as a formula of this type accurately describes the intensity pattern, measurements of the larger rings obtained yield a particle diameter that is more reliable than one made using smaller rings because the positions of the larger rings are less sensitive to changes in  $P$ .

A formula quite similar to equation (1) above, but based on Rodriquez' work<sup>(8)</sup> on the kinetic theory of fluids has been given by Fournet<sup>(9)</sup>:

$$I = M N^2 \Phi^2(u) \left[ 1 + (8v_0 v / v_1) \Phi(2u) \right]^{-1} \quad (2)$$

wherein  $v_0$  and  $v_1$  are the true and mean particle volumes, respectively, and  $\nu$  is nearly constant. The theoretical calculation of  $\nu$  requires a knowledge of the interaction potential between the particles so that except for relatively few cases<sup>(8)</sup>, it must be determined experimentally. One of the main assumptions underlying (2) is the supposition that the probability distribution function describing the particle positions does not differ markedly from  $e^{-\phi(r)/kT}$  where  $\phi(r)$  is the interaction potential between spheres. For particles as large as the latex spheres under consideration, the validity of this assumption may be questioned. Nevertheless, for large values of  $u$  (or small values of  $P$  and  $\nu v_0/v_1$ ), equations (1) and (2) become identical.

We have based our size determinations upon equation (1). Table II gives the values of  $u$  for which the intensity has a relative maximum for the cases  $P = 0$  and  $P = \frac{1}{2}$ . The calculation of these  $u$  values was made by use of the equation

$$a_n = \gamma b_n - 5P\gamma b_n^2/2 + \delta b_n^3 + \epsilon b_n^4 + O(b_n^5)$$

where:  $a_n = u_n - n\pi$

$$b_n = \frac{1}{n\pi}$$

$$\gamma = \frac{5P}{2} - 3$$

$$\delta = 6\gamma - \frac{81P}{4} - \frac{67}{2} P\gamma - (5P + 6)\gamma^2 + \frac{25}{4} P^2\gamma - \frac{7\gamma^3}{3}$$

$$\epsilon = \frac{335}{4} P^2\gamma - 15 P\gamma - 25 P^2\gamma^2 - 25 P\gamma^2 + \frac{85}{6} P\gamma^3 - \frac{5P\delta}{2}$$

This equation was obtained by series expansion of the transcendental

Table II

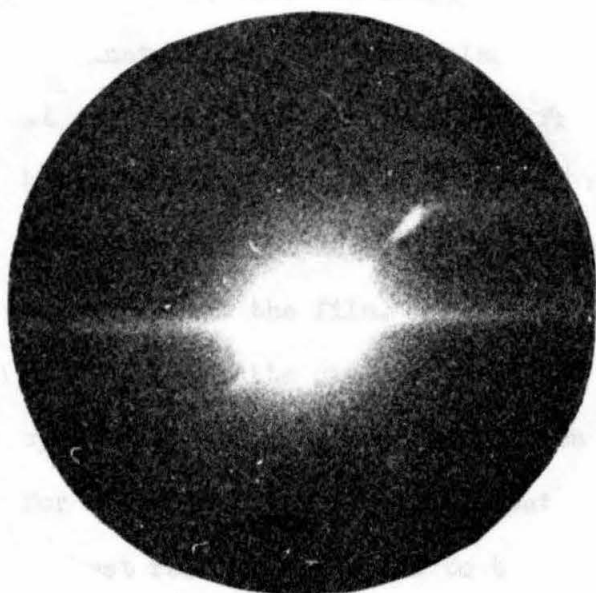
Peak Number	$u_{\max}$ (radians) for $P = 0$	$u_{\max}$ (radians) for $P = \frac{1}{2}$
5	15.515	15.602
6	18.689	18.761
7	21.854	21.915
8	25.013	25.066
9	28.168	28.215
10	31.320	31.362
11	34.471	34.509
12	37.619	37.654
13	40.767	40.799
14	43.914	43.944
15	47.060	47.088
16	50.206	50.235
17	53.351	53.375

equation connecting  $a_n$  and  $b_n$ , the final form being obtained by iteration of the resultant infinite degree algebraic equation.

The numbers in the columns to the right of the double line in Table I give the particle diameter inferred from the corresponding diffraction ring radius (for  $P = 0$ ) and the relative weight given to each measurement. (The results based upon equation (1) with  $P = \frac{1}{2}$  are given in Table IV).

#### Effect of Finite Size of Point Focus and Microphotometer Window

Probably the most important systematic error introduced into the above calculations, except possibly that due to inadequacies in the theory which yields equation (1), is the error which results from interpreting the data as though the primary beam converged to a mathematical point instead of the finite elongated spot used experimentally. Before describing the correction for this error, it is advantageous to consider the qualitative features of the primary beam. Fig. 8 shows two reproductions of exposures made, in the focal plane, with the primary X-ray beam. The 30 minute exposure shows the elongated nature of the point focus very clearly, while the longer exposure (31 hours) shows the magnitude and distribution of those much weaker parts of the primary radiation which are not focused in this elongated spot. All of the major features of the 31 hour exposure are readily explained: The streamer which makes an angle of about 45 degrees with the major axis of the focal spot is due to  $\text{Cu K}\alpha_1$  radiation that has been scattered (coherently but diffusely, i.e., not at the Bragg angle) by the first crystal in such a fortunate direction that it is subsequently focused (in a line) by the second crystal. The small spot which lies along the major axis of the focal spot about  $1 \frac{1}{2}$  mm from its center represents a "point focus" for the  $\text{Cu K}\alpha_2$  line, the



1.0 MM



1.0 MM

Fig. 8 On the left is shown a reproduction of a 31 hour exposure to the main beam at the "focal point", the major features of which are discussed in the text. The appearance of a film placed at the focal point and exposed for only 1/2 hour is shown at the right.

accompanying (very faint) streamer being due to  $\text{Cu K}\alpha_2$  radiation scattered by the first crystal and focused by the second. It is important to note that this non-Bragg reflected radiation has been completely eliminated from the focal plane except in two well defined regions where it can be readily distinguished from radiation scattered by the sample being studied. The true elongated nature of the main focal spot is somewhat obscured in the longer exposure. This is partially due to secondary scattering at the film.

The finite dimensions of the focal spot introduce an important systematic error in the diffraction ring diameters to a different degree for different azimuths of the pattern and different rings. The azimuth of best resolution normal to the long axis of the focal spot was the one invariably used for measuring ring diameters. Fig. 9 shows a map of the distribution of X-ray intensity over the focal spot as it was used for most of the latex work. The spot was divided into six annular sections or zones in such a way that the arcs defining these sections are concentric with the point of maximum intensity for a specified diffraction ring taken on the azimuth of greatest resolution, and the total direct beam intensity in each zone is assumed to be concentrated at the mid-point of the mean arc in that zone. Hence the effect of the true beam has been approximated by six ideal beams coming to a small array of true point foci along the azimuth of best resolution, an array which would yield essentially the same intensity distribution in the neighborhood of a given ring as that actually obtained. Finally, the radial position of the maximum expected for scattering from these six ideal beams is compared with the position of the maximum expected for a single central ideal beam. The corrections to the

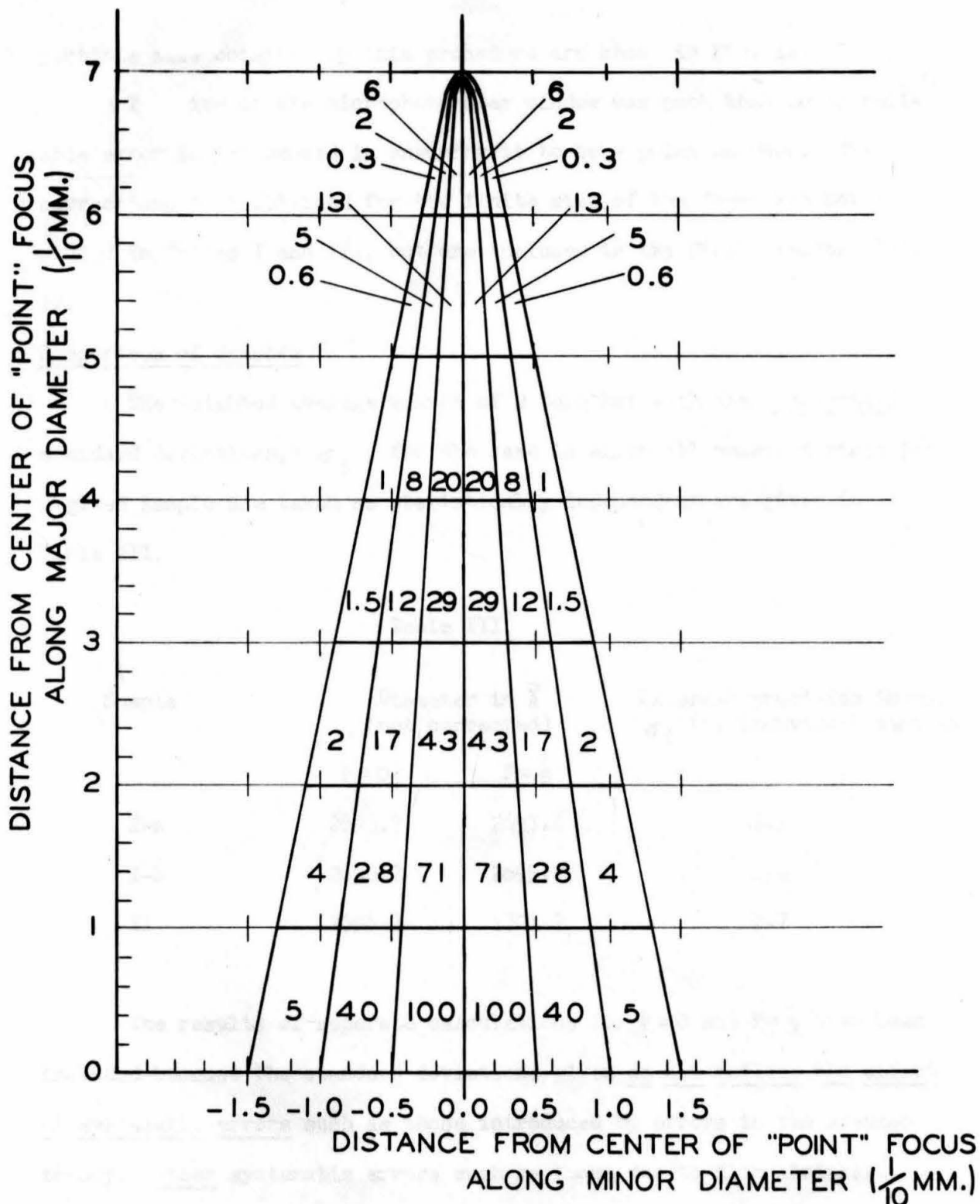


Fig. 9 This diagram shows the shape of half of the primary "point" focus, the other half being essentially the reflection of the part shown in the horizontal axis. The number in each subregion indicates the mean relative intensity there, as determined by microphotometer traces of a series of exposures made with the direct beam.

particle size obtained by this procedure are shown in Fig. 10.

The size of the microphotometer window was such that no appreciable error is introduced in assuming it to be a point scanner. The corrections just obtained for the finite size of the focus are not included in Tables I and III, but are included in the final results, Table IV.

#### Comparison of Samples

The weighted average values of  $D$  together with the statistical standard deviations,  $\sigma_i$ , for the case in which all measured rings for a given sample are taken as statistically independent are given in Table III.

Table III

Sample	Diameter in Å (not corrected)		External precision index, $\sigma_i$ (by individual samples)
	$P=0$	$P=\frac{1}{2}$	
I-a	2693.7	2697.6	2.0
I-b	2690.7	2695.9	2.4
II	2696.7	2701.7	2.7

The results of separate calculations for  $P=0$  and  $P=\frac{1}{2}$  have been included because the standard deviations given do not reflect the effect of systematic errors such as those introduced by errors in the assumed theory. Other systematic errors such as those due to film shrinkage, sample-to-film distance, and microphotometer distance calibration are believed to be less than  $2\frac{1}{2}$  Å (See evidence, Part III). Although systematic deviations of relative ring diameters from their theoretically

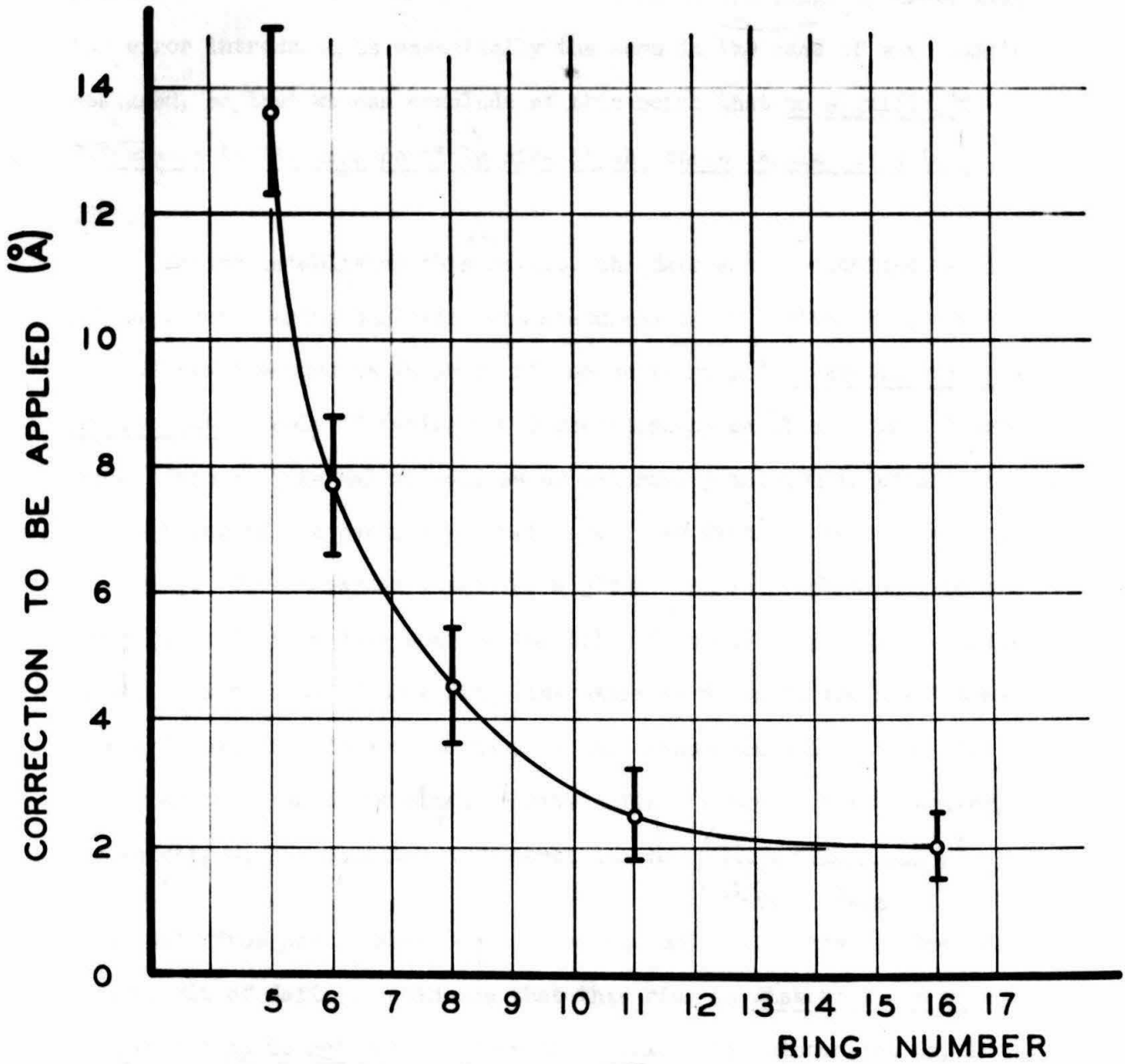


Fig. 10 Showing the correction to be applied to the diameter obtained from measurements of a given ring because of the finite size of the "point" focus.

predicted values still remain in the results at the stage of Table III, the error introduced is essentially the same in the case of each sample measured, so that we can conclude at this point that no significant difference in the mean particle size of the three samples used is indicated.

Having established this result, the data can be combined by ring numbers, considering the different measurements of a given ring (on all the different exposures in which it can be measured) as statistically independent. Table IV (using  $P=0$ ) presents the results of this treatment. Here an internal as well as an external precision index is attached to the value of the particle diameter obtained from all measurements of each ring. This internal index for a given ring is proportional to the reciprocal of the square root of the total (summed) weight of the individual measurements of this ring; the external index is the statistical standard deviation from their mean of the measurements involved. In combining the results by rings to give a final weighted mean diameter, the weight,  $W$ , has been taken proportional to  $\left( \frac{2}{\sigma_{int}^2 + \sigma_{ext}^2} \right)^{\frac{1}{2}}$ .

Also, data from peak number 8 has here been omitted. This has been done as a result of definite evidence that this ring is distorted due to radiation that is not scattered by the latex. This distortion is, in fact, due to the  $Cu K\alpha_2$  streamer referred to above in reference to Fig. 8. Fig. 11 shows a plot of inferred particle diameter versus the number of the intensity maximum whose position was used for the calculation, both for  $P=0$  and for  $P=\frac{1}{2}$ . In the case of  $P=0$ , there appears to be little, if any, suggestion of a decreasing diameter with higher order maxima,

Table IV

## COMPILATION OF DATA BY INDIVIDUAL MAXIMA

Number of Maximum	Number of Measurements Involved	$D_{P=0}(\text{\AA})$		$D_{P=\frac{1}{2}}(\text{\AA})$ Corrected	$\sigma_{\text{ext}}(\text{\AA})$	$\sigma_{\text{int}}(\text{\AA})$	W
		Uncorrected	Corrected				
5	9	2698.4	2684.8	2699.9	5.4	5.4	343
6	11	2703.9	2696.2	2706.8	3.7	3.6	750
7	12	2692.2	2686.4	2693.9	3.4	3.3	891
8	11	2711.2	2706.7	2712.4	5.5	3.3	(See Text)
9	10	2694.4	2690.9	2695.4	4.7	2.8	669
10	9	2687.2	2684.3	2687.9	2.3	3.2	1290
11	8	2690.3	2687.8	2690.8	2.2	3.2	1330
12	6	2692.5	2690.3	2692.8	2.8	3.3	1070
13	5	2690.7	2688.6	2690.7	3.2	4.1	739
14	3	2684.3	2682.2	2684.0	2.6	4.7	693
15	2	2686.6	2684.6	2686.2	1.5	5.9	540
16	2	2681.3	2679.3	2680.8	7.9	8.0	158
17	1	2686.8	2684.8	2686.0	-	13.0	59

Treating the above data as independent, one obtains:

$$\bar{D}_{P=0} = 2687.5 \text{ \AA} ,$$

$$\sigma_{\text{ext}} = 1.2 \text{ \AA}$$

$$\bar{D}_{P=\frac{1}{2}} = 2692.0 \text{ \AA} ,$$

$$\sigma_{\text{ext}} = 1.8 \text{ \AA}$$

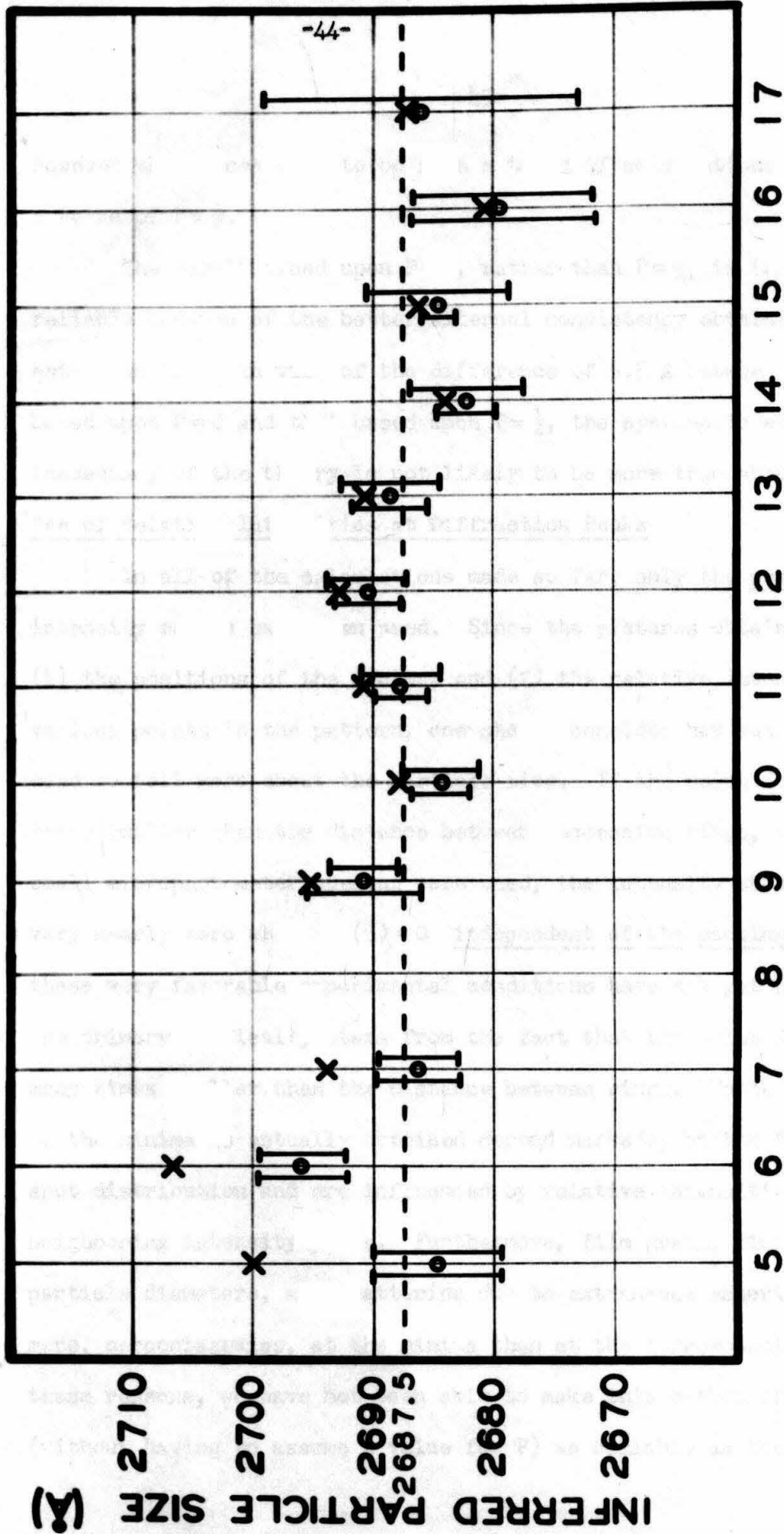


Fig. 11 This figure shows a plot of inferred particle diameters as a function of diffraction ring number as calculated from equation (1) both for P 0 (indicated by circles) and for P  $\frac{1}{2}$  (indicated by crosses). The lengths of the vertical lines on the left and right sides of the circles represent the external and internal precision indices respectively. These indices are the same for P  $\frac{1}{2}$  as for P 0. Ring number 8 has been omitted as explained in the text.

however there does seem to be such a trend if calculations are based on a value of  $P = \frac{1}{2}$ .

The result based upon  $P = 0$ , rather than  $P = \frac{1}{2}$ , is taken as the more reliable because of the better external consistency obtained, and it is estimated that, in view of the difference of  $5.5 \text{ \AA}$  between the value based upon  $P = 0$  and that based upon  $P = \frac{1}{2}$ , the systematic error due to inadequacy of the theory is not likely to be more than about  $7 \text{ \AA}$ .

#### Use of Relative Intensities at Diffraction Peaks

In all of the calculations made so far, only the positions of the intensity maxima have been used. Since the pictures obtained also yield (1) the positions of the minima, and (2) the relative intensity at various points in the pattern, one should consider how such data can be used to tell more about the particle size. If the point focus were many times smaller than the distance between successive rings, and a suitably small microphotometer opening were used, the intensity should drop to very nearly zero when  $\Phi(u) = 0$  independent of the packing. However, these very favorable experimental conditions have not yet been realized. The primary difficulty stems from the fact that the point focus is not many times smaller than the distance between rings. Hence the positions of the minima as actually obtained depend markedly on the "point focus" spot distribution and are influenced by relative intensities at the neighboring intensity peaks. Furthermore, film grain, finite range of particle diameters, and scattering due to extraneous material contribute more, percentagewise, at the minima than at the corresponding maxima. For these reasons, we have not been able to make this method of finding  $D$  (without having to assume a value for  $P$ ) as reliable as the one employing

the positions of the maxima and choosing P from the external consistency of the inferred values of D. The data obtained from the relative intensities at successive diffraction peaks is similarly complicated by the finite size of the point focus, but the agreement between the measured and predicted values for these relative intensities is fair. Here there is some evidence, however, that the intensities fall off somewhat faster for large values of u than formula (1) or (2) predicts. This can be accounted for by assuming that the latex particles do not have exactly the same size, but are distributed about a mean size (as is most certainly the case).

### Conclusions

Yudowitch's original measurements were made with the latex scattering sample in vacuum and he obtained a mean particle diameter of 2780 Å. Since that time, he has taken a new set of data with the scattering sample in air, this time obtaining a value of 2740 Å for the mean diameter. However, no significance was attached to the change from vacuum to air, the difference in the value obtained for the mean particle diameter being merely attributed to better technique in the case of the more recent measurements. This result (for latex particles in air) still differs from the above result of 2687.5 Å as the mean diameter of the latex spheres when under 1 atmosphere of helium (based on the assumption of random orientation) by more than twenty five times the statistical error in the latter and by about ten times the difference between the values found above for  $P=0$  and  $P=\frac{1}{2}$ . No systematic errors of this magnitude are believed to exist in the present work,\* but there seem to be at least two sources whereby

---

\* A separate experiment described in Part III shows that the latex particle size is very nearly the same for particles in vacuum as for particles under a pressure of 1 atmosphere of air or helium.

appreciable systematic error might enter into the measurements by Yudowitch. (1) Yudowitch used the Cr  $K\alpha$  line but isolated it from the rest of the spectrum by means of filters alone. His assumption therefore that the pattern was attributable to the Cr  $K\alpha$  radiation alone could introduce some error if his filtered beam contained enough radiation harder than the Cr  $K\alpha$  line. (2) Adequate importance when interpreting the diffraction pattern may not have been given to the effect of the finite extension of the primary beam. This last possibility seems most likely since no mention of such a correction was made in the paper describing the results, yet the resolution was not as good as that achieved with the point focusing monochromator.

### Part III

#### EFFECT OF EXTERNAL PRESSURE ON THE SIZE OF LATEX SPHERES

Most experimenters who have worked with the particle size determination of latex by X-ray diffraction methods have used techniques requiring the sample to be in vacuum. The original data obtained with the point focusing monochromator, however, were from scattering by a sample which was surrounded by a medium of helium at a pressure of one atmosphere. Comparison of these results with those obtained by Yudowitch (which were the only other X-ray diffraction results published at the time) placed the difference in the two values obtained for the particle diameter well outside the estimated probable error attached to either value. Since the diameter obtained by Yudowitch from particles in vacuum was larger than the value obtained in Part II (above) where the particles were in an atmosphere of helium, it was believed that part of the discrepancy might be attributed to particle dilatation with removal or reduction of pressure. Consequently an experiment was devised to measure this effect.

In view of the fact that small differences between two measurable quantities are invariably obtained with higher accuracy when measured directly than when taken as the difference between separate measurements, an effort was made to make the measurement of change in particle diameter with pressure as direct as possible. To this end, an airtight cell was designed to hold the latex sample and was provided with two mica windows about 0.007 inches thick and 7/8 inches in diameter through which the X rays could enter and leave the chamber without suffering excessive loss

due to absorption. Fig. 12 shows a schematic diagram of the cell while Fig. 13 is an actual photograph. As indicated in the diagram, the latex sample is supported at the center of the cell out of contact with the mica pressure windows by two 0.001 sheets of nylon (this substance being chosen for its very low absorption and scattering coefficients). The cell is placed at the usual sample position within the helium system, and a piece of pressure tubing, one end of which is connected to the cell, is led out of the system through a gas tight seal so that it can be attached to a vacuum pump or exposed to helium or air at atmospheric pressure as desired without requiring any movement of the sample. Since it is just the difference between the particle diameter in vacuum and in one atmosphere of helium or air that is to be found, one has much more freedom in choosing a method for obtaining appropriate data than was the case in Part II where the actual diameter was sought. The greatest freedom comes from the fact that systematic errors are here unimportant so long as they are the same when the particles are in vacuum as when they are in air or helium.

Two separate experiments were carried out to determine the sensitivity of the latex particle diameter to external pressure. The first experiment compared the diameter in vacuum to that in air, and was originally designed to detect diameter changes of the order of  $10 \text{ \AA}$ . When the results of this pilot experiment showed the change to be not more than about  $3 \text{ \AA}$ , a more careful experiment was devised. Since the best estimate of the particle dilatation with pressure makes use of the results of both experiments, they will be individually described below.

#### Vacuum-Air Experiment

The latex sample was put in the cell as described above. Six X-ray

exposures ranging from about 30 hours to 120 hours were made with the cell alternately evacuated and exposed to the atmosphere, the alternation being employed to minimize the effect of any changes which might occur at the X-ray focal spot during the course of the experiment.

In analyzing the diffraction patterns obtained, it was found that the usual microphotometering procedure (wherein an image of the film grain is formed on the window to the photocell) gave a microphotometer trace that was very sensitive to film grain in the low intensity region. In the case of the ring-like diffraction pattern of latex spheres, this difficulty could in principle be overcome by combining the results of microphotometer runs across several different diameters of the pattern. This tedious method can be justified only if (1) the scanning window used is small compared to the interesting detail of the pattern, and (2) the pattern (obtained with a finite beam of X rays) has circular symmetry. In order to obtain a similar smoothing effect and thereby render the microphotometer data from each exposure more useful, it was found advantageous to use the microphotometer in such a way that an image of the film grain is not formed at the window to the photocell; i.e., the film is placed slightly out of focus. The smoothing effect can then be alternately looked on as due to a Gaussian-shaped scanning window (the film being considered in focus) or due to a smearing of each grain in the film over a small region near that grain, the blackness decreasing as the distance from the grain is increased. Such a scheme is not normally useful when a true trace of the film density is required, and even the positions of intensity maxima will not in general be faithfully represented in the microphotometer trace obtained. This is because the regions on either side

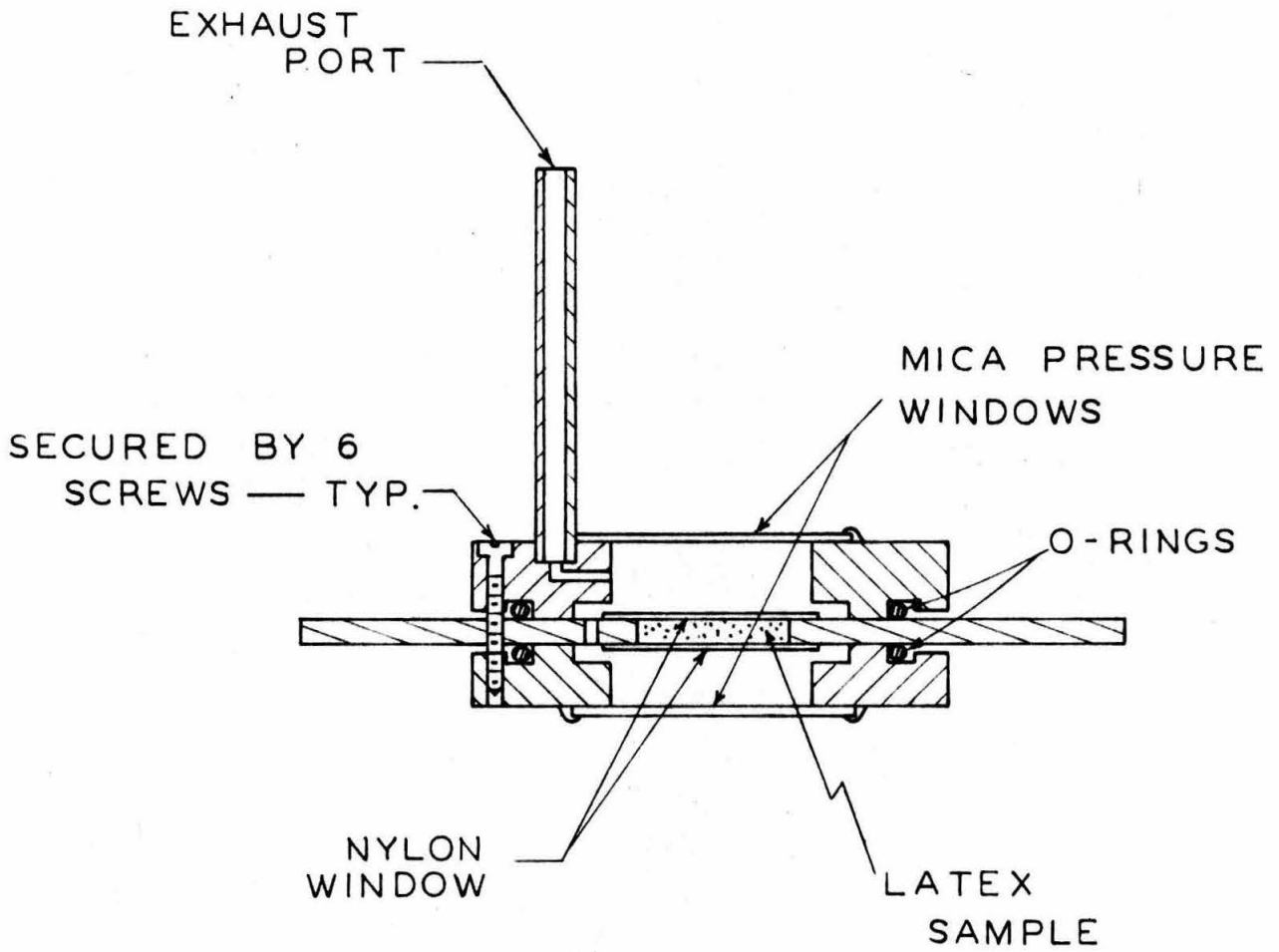


Fig. 12 Schematic diagram of the cell used for the vacuum-air and vacuum-helium experiments.



Fig. 13 Photograph of the cell used for the vacuum-air and vacuum-helium experiments.

of any maximum now contribute to the light received by the photocell even when the scanning window is centered over the maximum.

In the present case, the systematic error introduced by the use of such a (Gaussian) window should be the same for a ring in the diffraction pattern from particles in vacuum as for the corresponding ring from particles in air (it being assumed that the exposure times are nearly equal in the two cases). If, then, comparison of the particles in vacuum and in air is to be made ring by ring, an appropriate choice of the "scanning window" can be made (by adjusting the extent to which the film grain is out of focus) that will produce a smooth curve showing maxima and minima whose positions can be easily and accurately made. This window must, of course, be significantly smaller than the interesting detail of the diffraction pattern being studied.

In tabulating the results of ring measurements made from microphotometer traces obtained as described above, each ring measurement has been divided by the mean of all the measurements of that ring. The weight assigned to each of these ratios is then taken inversely proportional to the square of its estimated accuracy. Table V contains the pertinent data.

Calculations based on this table give

$$\left(\frac{R}{\bar{R}}\right)_{\text{Ave. for air}} - \left(\frac{R}{\bar{R}}\right)_{\text{Ave. for vacuum}} = 1.1 \times 10^{-3} \pm 0.43 \times 10^{-3}$$

where the accuracy estimate,  $\pm 0.43 \times 10^{-3}$  is made from the following considerations: The systematic error introduced by the microphotometer scanning window is certainly small, and should vary smoothly from ring to ring. Hence by dividing  $\bar{R}_n$  by  $u_n$  (Table II, Part I) and plotting this ratio

Table V

Exposure Number	Latex Surrounded By:	$1 - \frac{R_5}{\bar{R}_5}$	$w_5$	$1 - \frac{R_6}{\bar{R}_6}$	$w_6$	$1 - \frac{R_7}{\bar{R}_7}$	$w_7$	$1 - \frac{R_8}{\bar{R}_8}$	$w_8$	$1 - \frac{R_9}{\bar{R}_9}$	$w_9$	$1 - \frac{R_{10}}{\bar{R}_{10}}$	$w_{10}$
1.	Air	-0.0041	62	-0.0030	199	-0.0045	122	-0.0013	57	+0.0001	50	+0.0027	63
2.	Vacuum	+0.0065	62	+0.0015	199	-0.0064	68	-0.0088	157	-0.0013	200	+0.0054	63
3.	Air	+0.0012	62	+0.0003	199	+0.0051	122	+0.0004	157	-0.0015	50	-0.0092	35
4.	Vacuum	-0.0015	35	+0.0015	199	+0.0003	122	+0.0029	157	+0.0016	200	+0.0019	252
5.	Air	-0.0015	16	-0.0019	199	+0.0003	122	+0.0013	157	-0.0013	200	+0.0001	252
6.	Vacuum	-0.0068	224	+0.0015	199	+0.0022	122	+0.0054	157	+0.0046	200	+0.0021	142

$R_n$  = diameter of any ring number n

$\bar{R}_n$  = mean diameter of all rings number n

$w_n$  = weight corresponding to  $R_n/\bar{R}_n$

against  $n$ , a smooth curve which is nearly constant should result if the experimental mean,  $\bar{R}_n$ , were equal to the corresponding true mean,  $\bar{R}_n^*$ . Thus the smooth line that approximately fits the points  $\bar{R}_n/u_n$  is taken as the locus of points  $\bar{\bar{R}}_n/u_n$ . By approximating  $\bar{\bar{R}}_n$  in this way, the deviation of  $R_n$  (a single experimental value) from  $\bar{\bar{R}}_n$  is found. Finally, the standard deviations of  $\left(\frac{R}{\bar{\bar{R}}}\right)_{\text{Ave. for air}}$  and  $\left(\frac{R}{\bar{\bar{R}}}\right)_{\text{Ave. for vacuum}}$  are found by the usual statistical means. From these, the standard deviation of the difference is calculated and is found to be  $\pm 0.43 \times 10^{-3}$  as given above.

Translated into angstrom units, the foregoing result indicates that the mean particle diameter of latex spheres is about  $3 \text{ \AA}$  less in a medium of air (at one atmosphere) than in a vacuum.

The above procedure is subject to criticism on at least three points: (1) Variation in film shrinkage from film to film might cause apparent variations in particle size that are as great or greater than  $3 \text{ \AA}$ . (2) The exposure times were not the same on all the films used, hence the systematic error introduced in a given ring measurement by the Gaussian scanning window probably varies slightly from film to film. (3) Moisture from the air may significantly influence the results. The variation in film shrinkage is a random type of variable, and although exposure times varied from about 30 to 120 hours, the variation in the exposure times for particles in vacuum was nearly the same as for particles in air.

---

\* This true mean is the mean of an infinite number of measurements of the  $i^{\text{th}}$  ring and, of course, can never be exactly known.

Consequently the above experiment is sound with respect to the first two of these criticisms provided sufficient exposures are made. When the size change was found to be not more than about  $3 \text{ \AA}$ , it was nevertheless felt that the experimental technique should eliminate the uncertainties due to film shrinkage and unequal exposure time, and minimize the possible effect of water vapor.

#### Vacuum-Helium Experiment

To eliminate errors due to unequal film shrinkage, a means of exposing the film in two small dots about 0.005 inches in diameter and a known distance apart (1.1243 inches) was provided.\* The dots were placed far enough apart so that they would not interfere with the diffraction pattern from the latex. The pressure tube leading from the latex cell was connected to the helium system surrounding the X-ray path, and, since the water vapor content of the helium used is extremely low, this connection served a dual purpose by eliminating the possibility of extraneous effects due to water vapor, and by providing the latex particles with the same medium as that used for the work described in Part II.

Six 25 hour exposures were made and microphotometer traces obtained using the out-of-focus method described above. Because of the comparatively shorter exposure time used, fewer measurable rings were obtained, but the accuracy with which rings number 5 and 6 can be obtained is quite high so that the data nevertheless are very consistent. The essential data together with the inferred results are given in Table VI. Calculation of the change in particle size is made in essentially the same way as was done in the vacuum-air experiment (except that film shrinkage is now corrected for).

---

\* See Part VI for fuller description.

The notation is the same as that used in connection with Table V.

Table VI

Exposure Number	Latex Particles In:	$1 - \frac{R_5}{\bar{R}_5}$	$1 - \frac{R_6}{\bar{R}_6}$	Separation Between Calibration Spots (half-millimeters)
1.	Helium	-.0027	-.0009	57.01
2.	Helium	.0032	-.0021	57.01
3.	Helium	.0026	.0044	56.99
4.	Vacuum	-.0001	-.0015	57.00
5.	Vacuum	.0006	.0002	57.07
6.	Vacuum	-.0034	.0002	57.00

The microphotometer traces obtained were such that equal weights were attached to the ring numbers used (i.e., rings number 5 and 6). The results of calculations based on this table give

$$\left(\frac{R}{\bar{R}}\right)_{\text{Ave. for vacuum}} - \left(\frac{R}{\bar{R}}\right)_{\text{Ave. for helium}} = 1.4 \times 10^{-3} \pm 0.9 \times 10^{-3}$$

(The accuracy could be improved here by using longer exposures, which were not practicable at the time the exposures for Table VI were obtained.)

It should be noticed that film shrinkage is remarkably uniform, the maximum variation in length being about 0.1%.

### Conclusions

The results of the last two sections show that a measurable decrease

in particle size with an increase of 1 atmosphere in external pressure is definitely indicated. Using these results, one obtains a value of  $3.4 \times 10^{-3} \pm 1.4 \times 10^{-3} \text{ atm.}^{-1}$  as an estimate for the bulk modulus of individual latex spheres (which is rather large in comparison with the bulk modulus for most solids). The probable error in this result is, however, fairly high so that inferences made from the large bulk modulus obtained above should be carefully checked.

Since the extent of this decrease is of the same order of magnitude as the uncertainty in the mean particle diameter obtained in Part II, the results in that section are not seriously affected. Besides demonstrating the approximate sensitivity of latex particle size to pressure, the experimental technique described above shows that slight changes (of the order of 0.1%) in the size of any sample consisting of uniform spherical particles can be obtained from measurements of the X-ray diffraction pattern of that sample. Some rather fundamental biological problems for which this technique is especially suitable have been suggested and are discussed in Part VI.

Part IV

INVESTIGATION OF THE LOW ANGLE DIFFRACTION FROM ORIENTED COLLAGEN

Recent efforts, particularly by chemists and biologists, to discover the chemical structure of many of the amino acid compounds (believed to be nature's basic building blocks) have revealed, in particular, much information about collagen. <sup>(10)\*</sup> Quantitative chemical analysis has been made on collagens from such varied sources as ox-tendon, hide, swim bladder, and gelatin. The results of such analysis indicate that these collagens are essentially alike as regards the percentage in which a given element is present, and also as regards the constituent amino acids. Some differences such as varied solubility in dilute acids have, however, been noted.

Other information has been obtained by electron microscopy and through infra-red work. The electron microscope shows that collagen is, as its name implies, (except in the case of gelatin) actually made up of a multitude of small fibrils possessing what appears to be periodicities of about 400 to 1000 Å along the fibril axis, the period being essentially constant for a given fiber. It is also significant, as will be appreciated when X-ray data is presented, that these measured periodicities lie on a Gaussian curve with a most probable value of 644 Å. Certain fine structure within these large periodicities has also been observed. The infra-red information is largely confined to data which reveals the C=O bond to be

---

\* This report by R. A. Pasternak and R. B. Corey gives a complete summary of the work (through 1951) on the structure of collagen and includes references on all phases of the work. The introduction to Part IV makes free use of the material in this report.

preferentially oriented along the axis of the fibril.

A large amount of data has been obtained using X-ray diffraction techniques. These data fall rather naturally into two groups, one group from large-angle scattering and another from small-angle scattering. The former category includes scattering attributed to spacings of about 2.85, 9.21, and 4.03 Å, while the latter consists of scattering from what appears to be a one dimensional periodicity with a repeat distance of about 640 Å.

Although much work had been done, particularly by Bear and Bolduan<sup>(11,12)</sup> on the low angle diffraction of X rays by collagen previous to the development of the point focusing monochromator, it was felt that additional useful information concerning the large (640 Å) periodicity might be obtained through the use of the high resolution attainable with this instrument.

#### Sample Preparation

Since the collagen fibrils in kangaroo tail tendon are particularly well oriented, the fibril axes being quite parallel, this substance was used as the scattering sample. A piece of tendon about 3/32 inches in diameter and 4 inches long was supplied by Professor Corey of the Department of Chemistry. The tendon was soaked in water for several hours, then teased apart to obtain about 8 pieces of tendon of smaller diameter which were then stretched, clamped, and dried.

The scattering from collagen is optimum for a sample thickness of about 1 mm normal to the X-ray beam, and the crosssection of the beam at the sample position required for best resolution is almost 2 square cm. Since it is desirable to have the fibril axis normal to the X-ray beam

the final clamping device was designed to hold the appropriate layer of stiff rope-like pieces of tendon. An attempt was made to stretch the tendon by about ten percent of its original length so as to increase its orientation; however, the clamping requirements made it difficult to control the stretching accurately so the actual increase in length varied from about 5 to 15%. Fig. 14 shows the final mounting for this kangaroo tendon. It can be seen that the fibril axes make an angle of about  $45^\circ$  with the square hole which allows the X-ray beam to pass through the sample. This was done so as to make the direction of best resolution on the film be along the fibril axis (see page 11 for discussion of resolution adjustments).

Some stringiness could be observed in each piece of tendon, the "string" axis being nearly coincident with the long dimension of the tendon. The axes of the various pieces of tendon were not strictly parallel and coplanar, but the inclination of any axis with the mean sample plane was not more than about  $2^\circ$ , and the departure from parallelism in the mean plane was not more than  $4^\circ$ .

#### Diffraction Pattern Obtained and its Interpretation

The sample was placed 657.3 mm from the film in an atmosphere of helium gas and exposed to the converging X-ray beam of the point focusing monochromator for 329 hrs. A reproduction of the diffraction pattern obtained is shown in Fig. 15. The essential feature of the pattern is the series of short inclined lines located to the lower left and upper right of the dark central spot caused by the direct beam. (Other exposed portions on the film are the same as those described on page 36 in connection with the latex work and have no special significance in the present connection.)

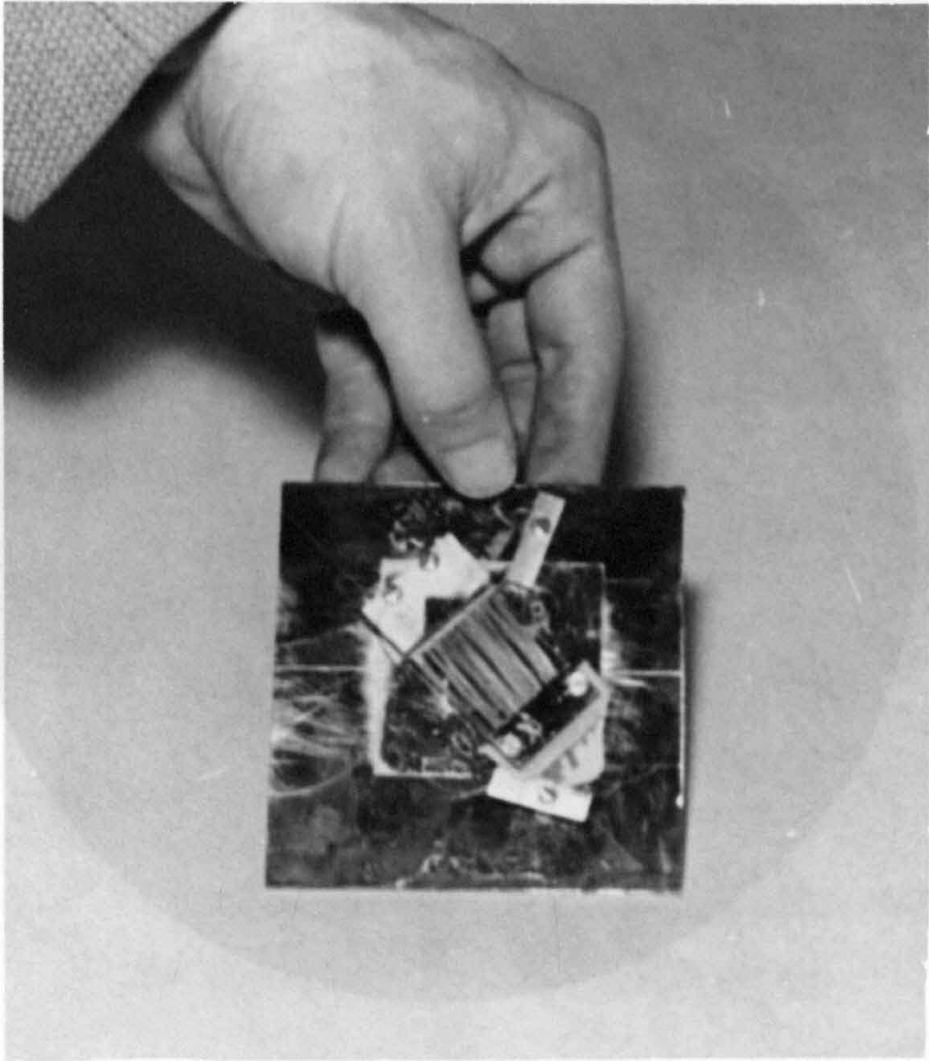


Fig. 14 Photograph showing the mounting of the kangaroo tail tendon for the study of scattering from oriented collagen.



Fig. 15 The diffraction pattern obtained from oriented kangaroo tail tendon.

As indicated above, such a series of lines had been previously obtained by other investigators, but the pattern obtained with the point focusing monochromator is superior to others in that, although it represents scattering from a very large number of non-uniformly stretched fibrils, even the first order lines are very clearly resolved. The high resolution is a result of the narrowness of the point focus and the very small wavelength spread in the radiation being scattered.

Quantitative data pertaining to the diffraction pattern (Fig. 15) is given in Table VII.

A meaningful interpretation of these data can best be given in terms of a cylindrical fibril model with axial periodicity, such as is suggested by electron microscope pictures of the fibrils. The mathematical details of theoretically predicting the low angle X-ray pattern expected from a cylinder with axial periodicity are conveniently formulated in terms of a reciprocal space, and have been given by Bear and Bolduan. (11, 1950) The relation between cylindrical coordinates in the scatterer and those in reciprocal space is shown in Fig. 16. Here  $\bar{s}_0$  is a unit vector in the direction of the unscattered beam, and  $\bar{s}$  is a unit vector in the direction in which scattering is to be observed (hence  $\bar{s}$  terminates in a spherical cap through the terminus of  $\bar{s}_0$  which, for low angle studies, may be taken as a plane). The origin of reciprocal space is designated by 0, and the vector  $\rho^* = \bar{s} - \bar{s}_0$  has reciprocal space cylindrical coordinates  $r^*$ ,  $\phi^*$ , and  $z^*$ . The line  $r^* = 0$  is parallel to the axis of the scattering cylinder, and the plane  $\phi^* = 0$  is coincident with the  $\phi = 0$  plane.

Using the notation of the figure, the above mentioned authors

Table VII

$d =$  Sample to film distance  $= 657.3 \pm 0.4$  mm

Size of main beam: length\*  $= 0.6$  mm; width\*  $= 0.14$  mm

$s_1 =$  1st order peak separation  $= 3.17 \pm 0.02$  mm

$s_2 =$  2nd order peak separation  $= 6.40 \pm 0.03$  mm

$s_3 =$  3rd order peak separation  $= 9.64 \pm 0.05$  mm

Width\* of 1st order peak  $= 0.16 \pm 0.01$  mm

Width of 2nd order peak  $= 0.17 \pm 0.02$  mm

Width of 3rd order peak  $= 0.17 \pm 0.02$  mm

Length\* of 1st order peak  $= 1.1 \pm 0.1$  mm

Length of 2nd order peak  $= 1.9 \pm 0.1$  mm

Length of 3rd order peak  $= 2.6 \pm 0.2$  mm

Relative intensity:

1st order peak, 76

2nd order peak, 12

3rd order peak, 5.3

\* Here and in the following discussion, the terms "length" and "width" (when applied to an elongated region which appears to have a major and a minor axis of symmetry) represent the distance between points where the intensity is just half as great as in the center of the region, these distances being measured along the major and minor axis, respectively.



show the intensity scattered toward the end of vector  $\rho^*$  for a circularly cylindrical scatterer of radius R with an axial electron density of periodicity  $b_0$  to be:

$$I_{\rho^*} = I_0 i_e (\pi R^2)^2 \left[ \frac{J_1 \left( \frac{2\pi}{\lambda} R r^* \right)}{\pi R r^* / \lambda} \right]^2 \frac{\sin^2 \left( \frac{\pi M b_0 z^*}{\lambda} \right)}{\sin^2 \left( \frac{\pi b_0 z^*}{\lambda} \right)} |F|^2 \quad (3)$$

wherein F is the density structure factor for one period along the axis,  $M = (\text{cylinder length})/b_0$ ,  $I_0$  is the incident intensity, and  $i_e$  is the intensity scattered by a single electron for unit incident intensity.

Since M is assumed large, the scattered intensity is limited to small regions or peaks about the planes  $z_k^* = \frac{k \lambda}{b_0}$  (where  $k = 0, 1, 2, \dots$ ) of reciprocal space. For purposes of seeing how well the experimental data given above matches this idealized theory, it is convenient to compare the theoretical expressions for the lengths and widths (as defined above) of the diffraction peaks with those experimentally observed. Bolduan and Bear show these distances to be approximately described by the equations:

$$\begin{aligned} \text{length}_k &= \frac{2 \lambda d}{\pi R} \sqrt{\ln 2} && \underline{\text{independent of } k} \\ \text{width}_k &= \frac{2 \lambda d \sqrt{\pi \ln 2}}{\pi M b_0} && \underline{\text{independent of } k} \end{aligned}$$

where d is the sample-to-film distance.

The difference in the lengths of the three experimental peaks is greater than would be expected if the difference in length were due only to angular spread in the fibril axes. (In this connection it is also significant that no curvature can be noted along the length of the

peaks.) However, refinement of the above theory to include the case where the ideal cylindrical fibril discussed above is replaced by a sheath of fibrils with small statistical lateral and longitudinal displacement of fibril parts ( 11, 1951) shows that such a sheath would give a diffraction pattern in which the peak lengths increase almost linearly with the peak numbers. The sheath radius cannot be found from these lengths unless the values of certain parameters describing the fibril distortion are known. These parameters are not amenable to direct measurement so that the peak lengths actually obtained will only be used to show agreement with the qualitative predictions of this model. With this model, as with the smooth cylinder model discussed above, the predicted peak widths are essentially constant.

Reference to Table VII shows that the widths of the peaks differ from the central beam width by only about 0.3 mm whereas the peak separation is as much as about 10 mm; hence these data offer very strong support to the assumption that there is truly a well defined axial periodicity in collagen tendon that varies only slightly from fibril to fibril. The magnitude of these variations in periodicity from the mean must be less than about 3% for the sample studied (this figure being the width difference over the peak separation), for misalignment or distortion of the fibrils would only increase the peak widths.

The process of drying a tendon whose normal biological environment is moist might well be expected to introduce considerable distortion into normally cylindrical fibril elements. The almost linear increase in peak width with peak number agrees with predictions of the above mentioned theory based on a sheath of distorted fibrils as a model, thereby lending

experimental evidence to support assumptions underlying the theory.

The relative intensities for the successive peaks from a smooth-cylinder fibril vary as the square of the fibril density structure factor,  $|F(z^*)|^2$  (see equation 3). Hence, insofar as such a model describes the true fibril structure, the gross behavior of  $F(z^*)$  can be found from the relative peak intensities.

Using the measured peak separations and sample-to-film distance, the axial periodicity can be found from the equation for the peaks:

$$b_0 = \frac{k \lambda}{z_k^*} = \frac{2k \lambda d}{s_k}$$

The results are:

Table VIII

Order number, k	$b_0$ (Å)	Weight
1	637.4	25
2	631.4	44
3	628.8	36

giving  $\bar{b}_0 = 631.9 \pm 2.3 \text{ Å}$

### Conclusions

As mentioned earlier, measurements of axial fibril periodicity by low angle diffraction have been made by other investigators, but this is the first work in which a large group of individually stretched fibrils have been used to obtain a single diffraction pattern, and the resolution is such that the ratio of peak width to peak separation is about 1 to 10

whereas other investigators have obtained only about a 1 to 1 ratio. Consequently the real contribution of the above work is the almost irrefutable evidence it gives to support the belief that the observed periodicity in the diffraction pattern is due to scattering from chain-like molecules with a definite structure that has a repeat distance of the order of 632 Å.

Although the exact structure of collagen is still unknown, Professor R. B. Corey believes that all of the data so far obtained on the collagens -- from large and small angle X-ray diffraction, electron microscope studies, chemical analysis, etc., -- can be explained in terms of a rather special chain-type molecule. The long dimension of the molecule would consist of two types of sections, every period in the axial structure containing one section of each type. One section, which accounts for the short periodicities of 10 Å and less, is made up of a helical carbon chain with various amino acid groups as residues. The other section has a much more complicated structure, probably due to the fact that proline rings, which are known to exist as such in collagen, have bonds with two carbon atoms thereby introducing distortions into the usual helical chain. These alternate spirals and knots would then account for the large repeat distance found above, and would explain the success of the cylindrical models mentioned above in explaining the gross features of the small angle pattern.

Part V

SCATTERING FROM IDENTICAL NONSPHERICAL PARTICLES  
RANDOMLY ORIENTED WITH APPLICATION TO BACTERIOPHAGE T-4

Thus far, only scattering due to spherical particles has been treated in detail. As an example of the quantitative information on particle size that can be obtained from X-ray scattering from a large class of more complicated particles whose general shape is known (say from electron microscopy), one may consider the scattering from identical particles whose shape may be approximated by two connected spheroids. In the treatment below, the case of random particle orientation will be assumed. This is probably the most useful assumption to make because particles whose shape can be suitably approximated by two spheroids occur most commonly as biological organisms in a suspending medium where the orientation tends to be random.

X-Ray Diffraction Pattern From Two Spheroids

Let the two spheroids comprising the particle whose diffraction pattern is to be found have their centers along a radius vector in a spherical polar coordinate system as shown in Fig. 17. The origin of the coordinate system is taken at the center of one of the spheroids, and the distance from the origin to the center of the other spheroid is designated by the letter  $l$ . Consider X rays scattered through a small angle  $\epsilon$ , and let the incident and scattered X-ray beam lie in the  $\phi = 0$  plane such that the bisector of the angle of deviation of the beam has a direction  $\phi = 0$ ,  $\theta = \pi/2$ . (Hence the "planes of reflection" are parallel to the equatorial plane of the spherical polar coordinate system.) To complete

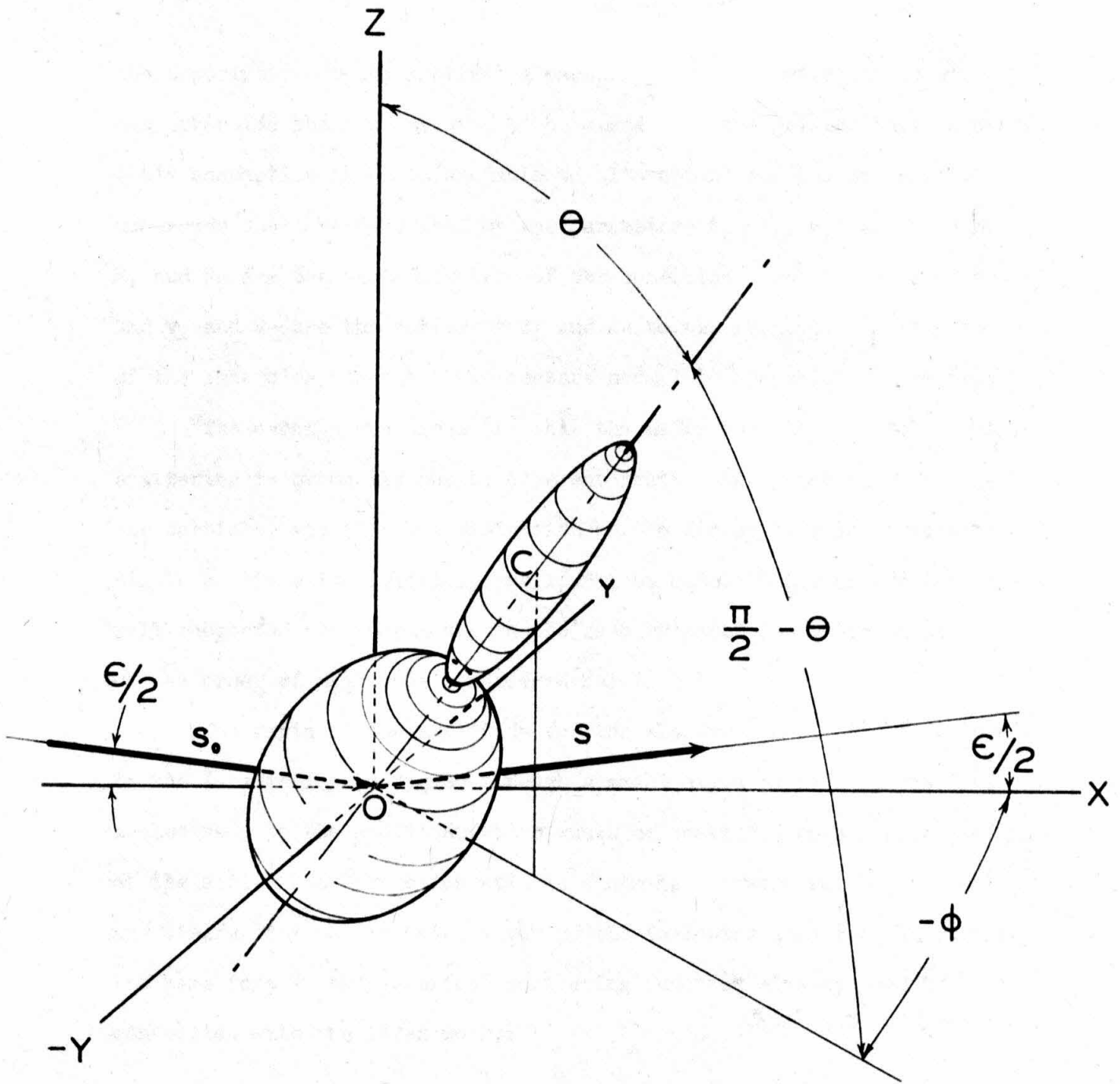


Fig. 17 Showing the coordinate system used in finding the radiation for randomly oriented particles consisting of two spheroids.

the description of the scattering particle, the axes of rotation of the spheroids shall be assumed to be along the line joining their centers (this assumption is quite amenable to alteration) and the sizes of the spheroids shall be described by the parameters  $R_1$ ,  $v_1$ ,  $R_2$ , and  $v_2$  where  $R_1$  and  $R_2$  are the semi-diameters of the spheroids along the axis of symmetry, and  $v_1$  and  $v_2$  are the ratios of  $R_1$  and  $R_2$  to the respective semi-diameters of the spheroids through their centers normal to the axis of symmetry.

The usual assumptions (1) that the major contribution to low angle scattering is primarily due to coherent scattering by the electrons in the particle, and (2) that diminution of the direct beam in traversing a single particle is negligibly small, will be made. These assumptions are well supported by experiments in the case of particles whose sizes are of the order of magnitude considered below.

The ratio of the amplitude for the electromagnetic field vectors of the X-radiation scattered through a small angle  $\epsilon$  by a spheroid of  $n$  electrons to the amplitude which would be scattered by a single electron at the center has been calculated in a straightforward way by Guinier<sup>(13)</sup> and others, the result being given by the following equation (which has the same form as the spherical scattering function already used in connection with the latex work):

$$\frac{A}{A_e} = n \frac{3}{u^3} (\sin u - u \cos u) \equiv n \Phi(u) \quad (4)$$

The symbols have the following significance:

$A$  and  $A_e$  are amplitudes scattered by the entire spheroid and a single element of volume respectively.

$$u = \frac{2\pi \epsilon R}{\lambda} \sqrt{\sin^2 \psi + v^2 \cos^2 \psi} \quad (5)$$

$R$ ,  $\epsilon$ ,  $n$ , and  $v$  have been defined just above.

$\lambda$  is the X-ray wavelength.

$\psi = \pi/2 - \theta$  is the angle between the axis of symmetry of the spheroid and the "planes of reflection" for the X rays under consideration.

The amplitude scattered by the particle (composed of two spheroids) can then be written

$$A = A_1 + A_2 e^{i \frac{2\pi \epsilon l}{\lambda} \cos \theta} \quad (6)$$

where use has been made of the vector properties of complex numbers. Since the total amplitude scattered from a body that is symmetric with respect to reflections through its center has the same phase as the radiation scattered by a small element at the center, the phase of the radiation from the second spheroid differs from that from the first by just  $\frac{2\pi \epsilon l}{\lambda} \cos \theta$  radians as given in equation (6).

The intensity scattered by a collection of identical particles with random orientation can now be obtained by superposing the intensities from all the particles; hence, by squaring the total scattered amplitude for a single particle and integrating over all particle orientations, the resultant intensity pattern for the collection can be found:

$$\begin{aligned}
 I &= K \int_0^{2\pi} \int_0^{\pi} \left( A_1 + A_2 e^{i \frac{2\pi \epsilon l}{\lambda} \cos \theta} \right) \left( A_1 + A_2 e^{-i \frac{2\pi \epsilon l}{\lambda} \cos \theta} \right) \sin \theta \, d\theta \, d\phi \\
 &= K \int_0^{2\pi} \int_0^{\pi} \left( A_1^2 + A_2^2 + 2A_1 A_2 \cos \left( \frac{2\pi \epsilon l}{\lambda} \cos \theta \right) \right) \sin \theta \, d\theta \, d\phi \quad (7) \\
 &= I_1 + I_2 + 2K \int_0^{2\pi} \int_0^{\pi} A_1 A_2 \cos \left( \frac{2\pi \epsilon l}{\lambda} \cos \theta \right) \sin \theta \, d\theta \, d\phi
 \end{aligned}$$

Here  $I_1$  and  $I_2$  are the intensities which would be scattered, respectively, by collections of randomly oriented spheroids of the two sizes composing the whole particle under consideration. The third term involves the phase relation between the two spheroids comprising a single particle. Series solutions for  $I_1$  and  $I_2$  in the form of a generalized hypergeometric function have been given by Roess and Shull.<sup>(4)</sup> However, a closed form solution has not been found, and the series does not converge rapidly in the present region of interest. Moreover, the integration of the term involving the phase relation between the spheroids gives rise to still another type of series which also converges slowly for values of  $u$  greater than a few radians. For these reasons, it has been found expedient to perform the integration by a combination of graphical and numerical procedures which will be outlined below. Because of the presence of a large number of parameters in equations (7), it is at this point inconvenient (and virtually impossible) to perform the indicated integration by graphical or numerical means. Consequently the general problem of finding the scattering from a collection of compound particles composed of two connected

spheroids will now be made more specific in that a specific particle shape will now be assumed. (The method employed below still remains quite general, however.)

#### Application to Particle Size Determination of Type T-4 Bacteriophage

Before describing the procedure for performing the integration of equation (7) when the particle shape is known, a digression on the bacteriophage particles to which the results will be applied is in order.

Many particles with sizes appropriate for study with the point focusing monochromator are of current interest to the biologist. As a large class of such particles, bacteriophage is especially suited to such size analysis because all of the particles of a given type have very nearly the same size and shape, thus avoiding the complication of size distribution. Several interesting and fundamental uses for the point focusing monochromator have been proposed in connection with measurements of phage size, some of which involve diffraction from phage of spherical shape (see Part VI). These applications necessitate a wet sample, and because no work with such a sample had actually been undertaken with the present instrument, a (successful) attempt was made to obtain the low angle diffraction pattern of the most readily available phage sample which happened to be type T-4. Using the point focusing monochromator, the sample size required for optimum scattering at high resolution is about 0.4 cc, so that sample preparation consists of starting with several liters of the dilute bacteria solution in which the phage can multiply and eventually concentrating the phage solution by centrifugation.

The external shape of T-4 has been determined using dry samples on collodion film in electron microscopes, so that it is reasonable to assume

that the shape of the particles is the same when wet as when dry, although the size may be appreciably different due to swelling.

Using electron microscope data on T-4 size when dry, <sup>(14)</sup> the parameters involved in approximating the true particle shape by two coaxial spheroids are as follows:

$$\frac{R_1}{R_2} = 4/5 \qquad v_1 = 3/2$$

$$\frac{R_1}{l} = 4/9 \qquad v_2 = 5$$

giving  $v_1 = \frac{16}{27} \pi R_1^3$

$$v_2 = \frac{5}{48} \pi R_1^3$$

On substituting these values into equations 4, 5, and 7, the intensity dependence of the radiation in the diffraction pattern on  $\epsilon R_1$  becomes

$$\frac{I}{I_e} = k \int_0^\pi \int_0^{2\pi} \left| \Phi(u_1(\theta)) + \frac{27 \times 5}{16 \times 48} \Phi(u_2(\theta)) e^{i 9.198 R_1 \epsilon \cos \theta} \right|^2 \sin \theta d\theta d\phi \quad (8)$$

where

$$u_1 = \frac{2\pi}{\lambda} \epsilon R_1 \sqrt{\cos^2 \theta + \frac{9}{4} \sin^2 \theta} = 4.09 \epsilon R_1 \sqrt{\cos^2 \theta + \frac{9}{4} \sin^2 \theta}$$

$$u_2 = \frac{2\pi}{\lambda} \frac{5}{4} \epsilon R_1 \sqrt{\cos^2 \theta + 25 \sin^2 \theta} = 5.11 \epsilon R_1 \sqrt{\cos^2 \theta + 25 \sin^2 \theta}$$

and  $R_1$  is in  $\text{\AA}$ .

The integration with respect to  $\phi$  can be performed immediately, and merely changes the constant in front of the integral. The problem, then, is to evaluate the integral over  $\theta$  from 0 to  $\pi$ , or over  $\cos \theta$  from -1 to 1. Furthermore, the integrand is even with respect to  $\cos \theta$ , hence integration from  $\cos \theta = 0$  to  $\cos \theta = 1$  will suffice. To accomplish this last mentioned integration, values of the integrand for a certain value of  $\epsilon R_1$  and a series of values of  $\cos \theta$  were obtained by a graphical method:  $\frac{u_1}{R_1}$  and  $\frac{u_2}{R_1}$  were plotted against  $\cos \theta$ , and a plot of  $\bar{\Phi}(u)$  vs  $u$  was also made. Then by use of proportional dividers whose ratio setting was equal to  $\epsilon R_1$ , values of  $u_1$  and  $u_2$  corresponding to any selected value of  $\cos \theta$  could be quickly obtained so that  $\bar{\Phi}(u_1)$  and  $\bar{\Phi}(u_2)$  were also readily found. Next, the phase difference,  $9.20 R_1 \epsilon \cos \theta$ , was found and  $\bar{\Phi}(u_1)$  and  $\bar{\Phi}(u_2)$  added vectorially, the length of the resultant being squared (graphically by use of a parabola) to give the value of the integrand. Finally, the value of the integrand obtained in this way was plotted against  $\cos \theta$ , the area under the resulting curve being proportional to the intensity associated with the particular value of  $\epsilon R_1$  used. Numerical methods (Simpson's rule and Weddle's rule) were used in evaluating this area, but the graph was nevertheless very useful in making a selection of the appropriate points to be used in the numerical integration.

A plot of  $I$  vs  $\epsilon R_1$  obtained in this way is shown in Fig. 18. This is the intensity pattern to be expected for scattering from bacteriophage T-4 when the direct X-ray beam converges to a true point. To obtain the approximate pattern to be expected for the finite focus actually used, this focus was approximated by five point foci. In choosing the appropriate

THEORETICAL INTENSITY CURVE  
FOR CASE OF IDEAL POINT FOCUS

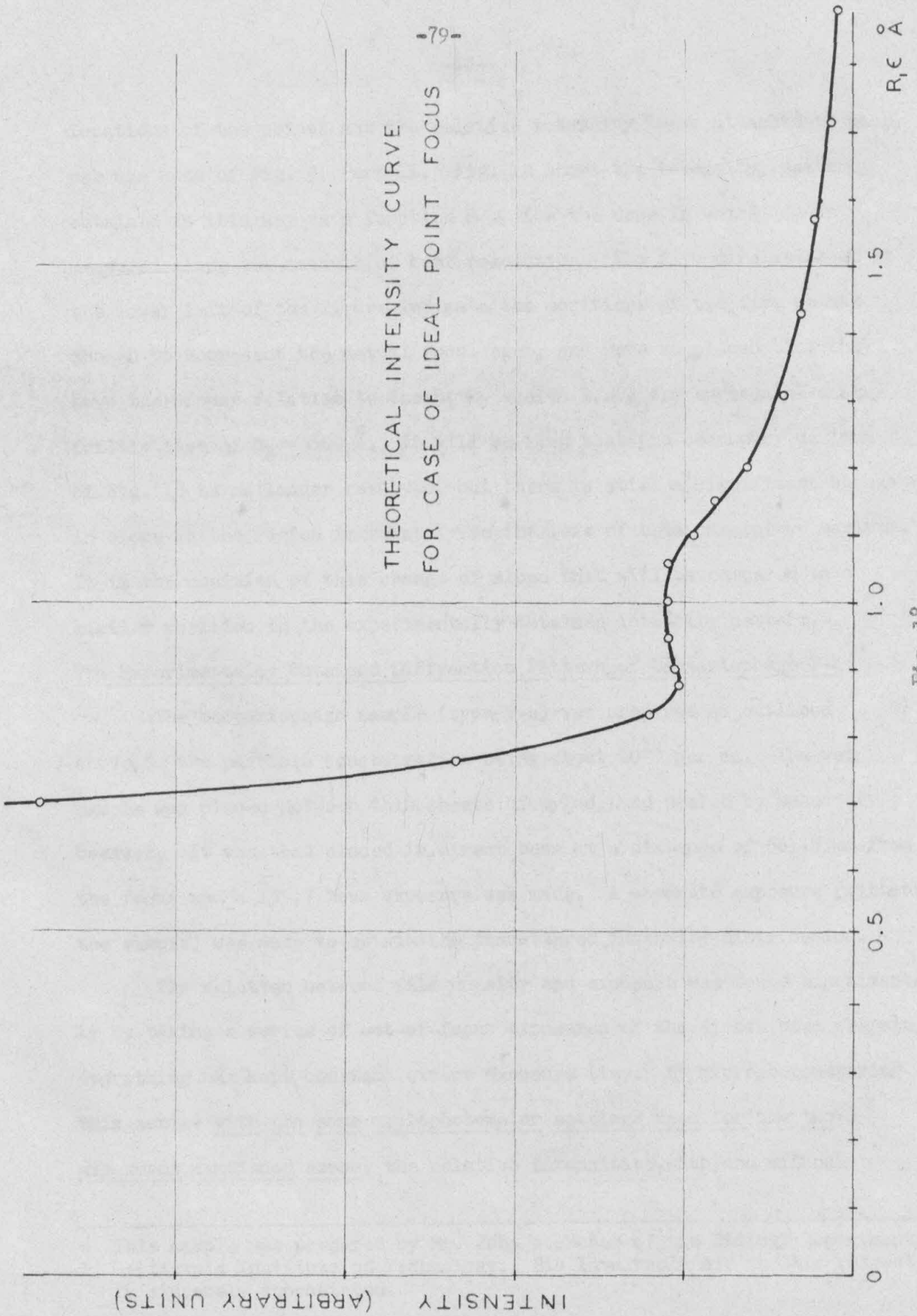


Fig. 18

locations of the points and the relative intensity to be attached to each, use was made of Fig. 9, Part II. Fig. 19 shows the intensity, pattern obtained in this way as a function  $R_1 \epsilon$  for the case in which  $\epsilon$  is measured along the azimuth of best resolution. The five circles shown at the lower left of the figure indicate the positions of the five points chosen to represent the actual focal spot, and were so placed that they have the proper relation to the  $R_1 \epsilon$  scale (i.e., the horizontal scale) for the case of  $R_1 = 600 \text{ \AA}$ . It will be seen that the secondary maximum of Fig. 18 is no longer resolved, but there is still a significant change in slope in the region immediately to the left of this unresolved maximum. It is the position of this change of slope that will be compared to a similar position in the experimentally obtained intensity pattern.

#### The Experimentally Obtained Diffraction Pattern of Bacteriophage T-4

The bacteriophage sample (type T-4) was prepared as outlined above,\* the particle concentration being about  $10^{11}$  per cc. The wet sample was placed between thin sheets of nylon, and sealed by means of beeswax. It was then placed in <sup>the</sup> direct beam at a distance of 661.8 mm from the focus and a 135.7 hour exposure was made. A separate exposure (without the sample) was made to obtain the unscattered intensity distribution.

The relation between film density and exposure was found experimentally by taking a series of out-of-focus exposures of the direct beam wherein everything was kept constant except exposure time. By microphotometering this series with the same microphotometer settings used for the two exposures mentioned above, the relative intensities with and without

---

\* This sample was prepared by Mr. John W. McKee of the Biology Department, California Institute of Technology. His invaluable aid in this respect is sincerely appreciated.

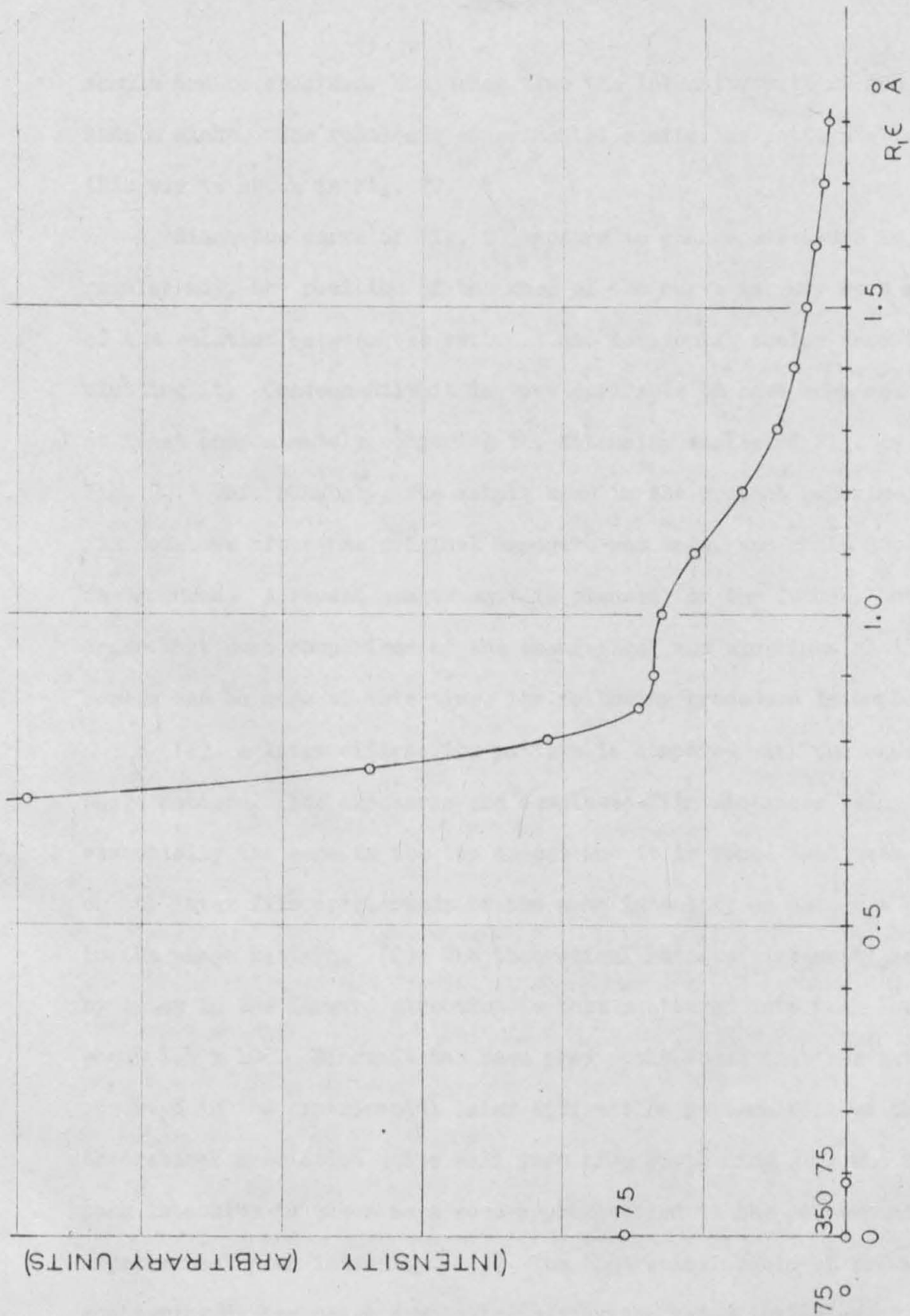


Fig. 19 Intensity versus  $R_1 \epsilon$  for the case in which the main beam consists of 5 ideal beams coming to point foci as explained in the text.

sample can be obtained, and hence also the intensity pattern due to the sample alone. The resultant experimental scattering pattern obtained in this way is shown in Fig. 20.

Since the curve of Fig. 20 appears to change curvature in a very regular way, the position of the knee of the curve is very much a function of the relation between the vertical and horizontal scales used in plotting it. Consequently it is very desirable to have some means of at least approximately comparing the intensity scales of Fig. 19 and Fig. 20. Unfortunately, the sample used in the present experiment lost its moisture after the original exposure was made, and could not be resuspended. A repeat measurement is planned for the future, but in order that some comparison of the theoretical and experimental intensity scales can be made at this time, the following procedure is employed:

(1) A latex diffraction pattern is compared with the experimental phage pattern, (the exposures and sample-to-film distances being essentially the same in the two cases) and it is found that peak No. 9 on the latex film corresponds to the same intensity as does  $\epsilon = 1.3 \times 10^{-3}$  in the phage pattern. (2) The theoretical ratio of intensity scattered by latex in the forward direction to that scattered into peak No. 9 is about  $1.4 \times 10^5$ . Since it has been previously found that the intensity observed in the experimental latex diffraction pattern follows the theoretical prediction quite well from ring #5 to ring #10, the theoretical peak intensity is taken as a good approximation to the corresponding experimental peak intensity. (3) The theoretical ratio of forward scattering by the phage sample to that by the latex (using equal exposures) is assumed to hold so that, using (1) and (2), the intensity corresponding

to  $\epsilon = 0$  in Fig. 20,  $I_0(20)$ , can be found in terms of the intensity at  $\epsilon = 1.3 \times 10^{-3}$  in the same figure.

$$\frac{\text{Forward scattering by phage sample}}{\text{Forward scattering by latex sample}} = \frac{t_P}{t_L} \frac{V_P}{V_L} \left( \frac{\rho_P}{\rho_L} \right)^2$$

where  $t_{P,L}$  = thickness of phage and latex samples, respectively

$V_{P,L}$  = volume per particle

$\rho_{P,L}$  = difference between electron density in the particle and that in the surrounding medium

In view of the foregoing considerations,

$$I_0(20) = 1.1 \times 10^3 \left( \frac{\rho_P}{\rho_L} \right)^2 I_{1.3}(20)$$

where  $I_{1.3}(20)$  is the intensity at  $\epsilon = 1.3 \times 10^{-3}$  in Fig. 20. The electron density in phage is about 1.1 to 1.2 times that in water, hence  $I_0(20) = (11 \text{ to } 44) I_{1.3}(20)$ .

The intensity corresponding to  $\epsilon = 0$  in Fig. 19 is about 40 times that at  $\epsilon R_1 = 0.7 \text{ \AA}$ . By comparing the vertical scale in Fig. 20 (throughout the uncertainty given above) with that in Fig. 19, it is possible to find the value of  $R_1$  which gives the best matching of the two curves (for each relation between the two vertical scales).

Values for  $R_1$  obtained in this way range from 390  $\text{\AA}$  to 540  $\text{\AA}$ , the two curves being most compatible for  $R_1 = 500 \text{ \AA}$ ,  $\frac{\rho_P}{\rho_L} = 0.1$ . Other possible values for  $R_1$  in the range from 390 to 540  $\text{\AA}$  cannot, however, be ruled out by the present experiment. The corresponding electron

microscope value is  $400 \pm 80 \text{ \AA}$  so that there is some suggestion of particle shrinkage with drying. In determining the "best match" between curves, only slight importance was given to the goodness of fit in the neighborhood of the kink in Fig. 19. Factors such as particle size distribution and shape variations might easily account for the fact that the experimental curve does not show this kink.

In summary, the need for another experiment to give the intensity corresponding to smaller values of  $\epsilon$  should be emphasized. It is believed by the author that such additional data will justify the assumptions regarding the comparison of intensity scales above and perhaps show more conclusively whether or not there is an appreciable change in particle volume during desiccation.

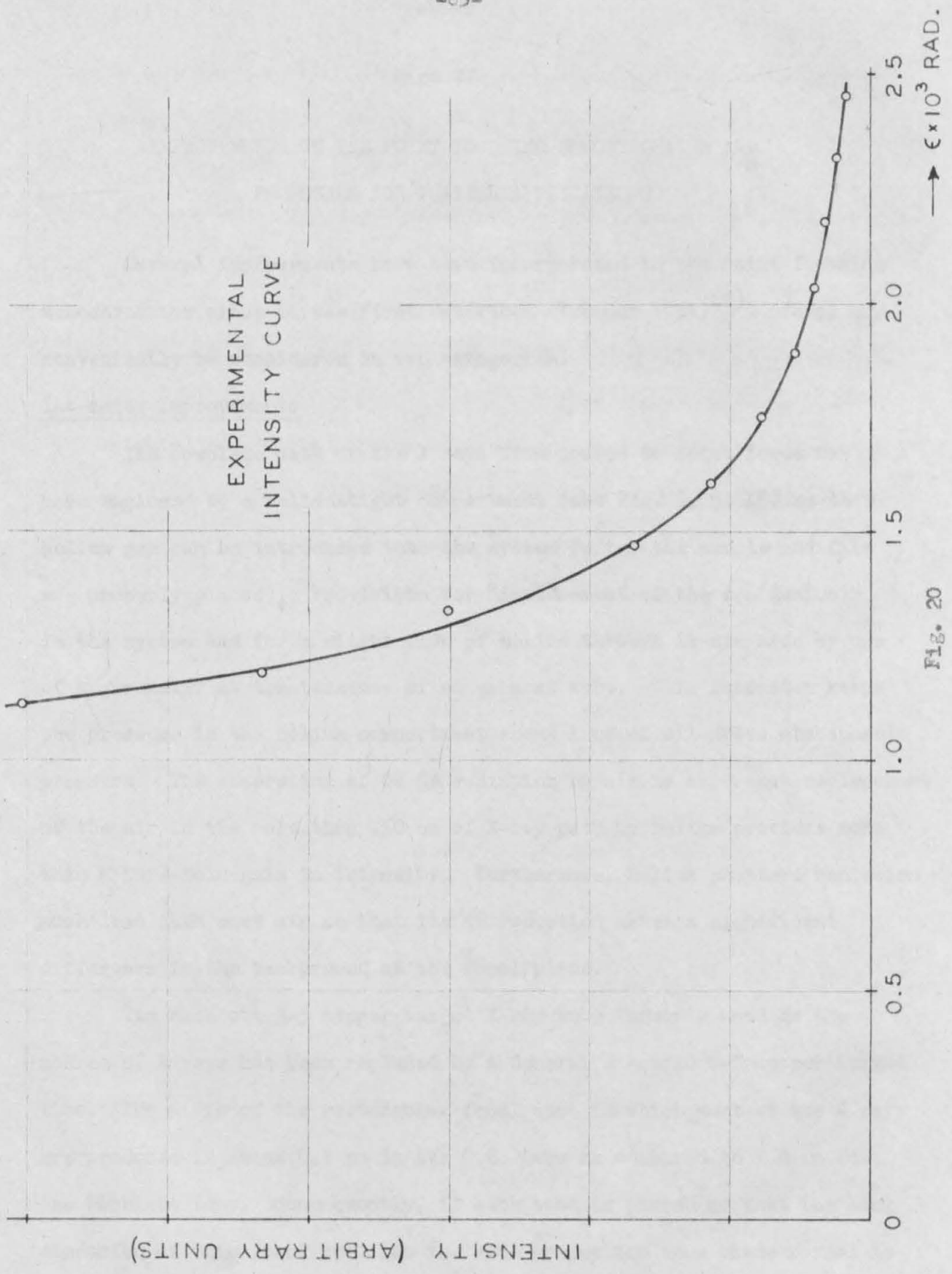


Fig. 20

Part VI

IMPROVEMENTS IN THE POINT FOCUSING MONOCHROMATOR AND  
PROPOSALS FOR FURTHER APPLICATIONS

Several improvements have been incorporated in the point focusing monochromator since it was first described (summer 1951)<sup>(2)</sup>. These may conveniently be considered in two categories.

Intensity Improvements

The complete path of the X rays from source to point focus has been enclosed by a helium-tight compartment (see Fig. 3, p. 15) so that helium gas can be introduced into the system (after the sample and film are properly placed). Provisions for displacement of the residual air in the system and for a slight flow of helium through it are made by use of a gasometer at the terminus of an exhaust tube. This gasometer keeps the pressure in the helium compartment about 1 cm of oil above atmospheric pressure. The absorption of Cu K $\alpha$  radiation by air is such that replacement of the air in the more than 150 cm of X-ray path by helium provides more than a threefold gain in intensity. Furthermore, helium scatters radiation much less than does air so that its introduction makes a significant difference in the background at the focal plane.

The Machlett A-3 copper target X-ray tube formerly used as the source of X rays has been replaced by a General Electric C-7 copper target tube. The width of the rectangular focal spot in which most of the X rays are produced is about 0.7 mm in the G.E. tube as compared to 1.0 mm for the Machlett tube. Consequently, if each tube is placed so that the long dimension of this focal spot has the same projection on a plane normal to

the central beam (going to the first crystal of the point focusing monochromator), and if the tubes are operated at the same current and voltage, the G. E. tube should have greater luminance over the central region of the projected focal spot than does the Machlett. Since, as shown in Part I, the main beam intensity is proportional to target luminance, an intensity gain of about 1.4 might be expected. Actually a somewhat greater gain (about 1.7) was obtained as a result of making this change in tubes. Since the tubes were operated at the same current and voltage, this surplus gain must be accounted for by assuming greater absorption of Cu  $K\alpha$  radiation in the target and/or the window of the older tube than in the new one. A slight tungsten deposit from the cathode onto the window of the old tube (operated more than 2500 hours) would explain such a difference.

In mounting the new tube (see Fig. 21), provision was made for adjustments which make it possible to incline the tube at about  $45^\circ$  with the horizontal so that the smaller dimension of the tube focal spot can be made parallel to the long dimension of the useful diagonal strip. Further adjustments allow one to choose the angle with which those rays that can be accepted by the monochromator leave the target. It is this latter adjustment that changes the luminosity of the target as viewed along the central ray to the monochromator.

There are still other means of increasing the intensity in the direct beam while maintaining the present high resolution of the instrument: (1) The quartz crystals could be replaced by topaz crystals so as to give a smaller Bragg angle, thus reducing the losses by unfavorable polarization of the reflected radiation. (2) The reflecting surfaces of the quartz crystals could be "roughened" a slight amount. (3) The "webs" which span

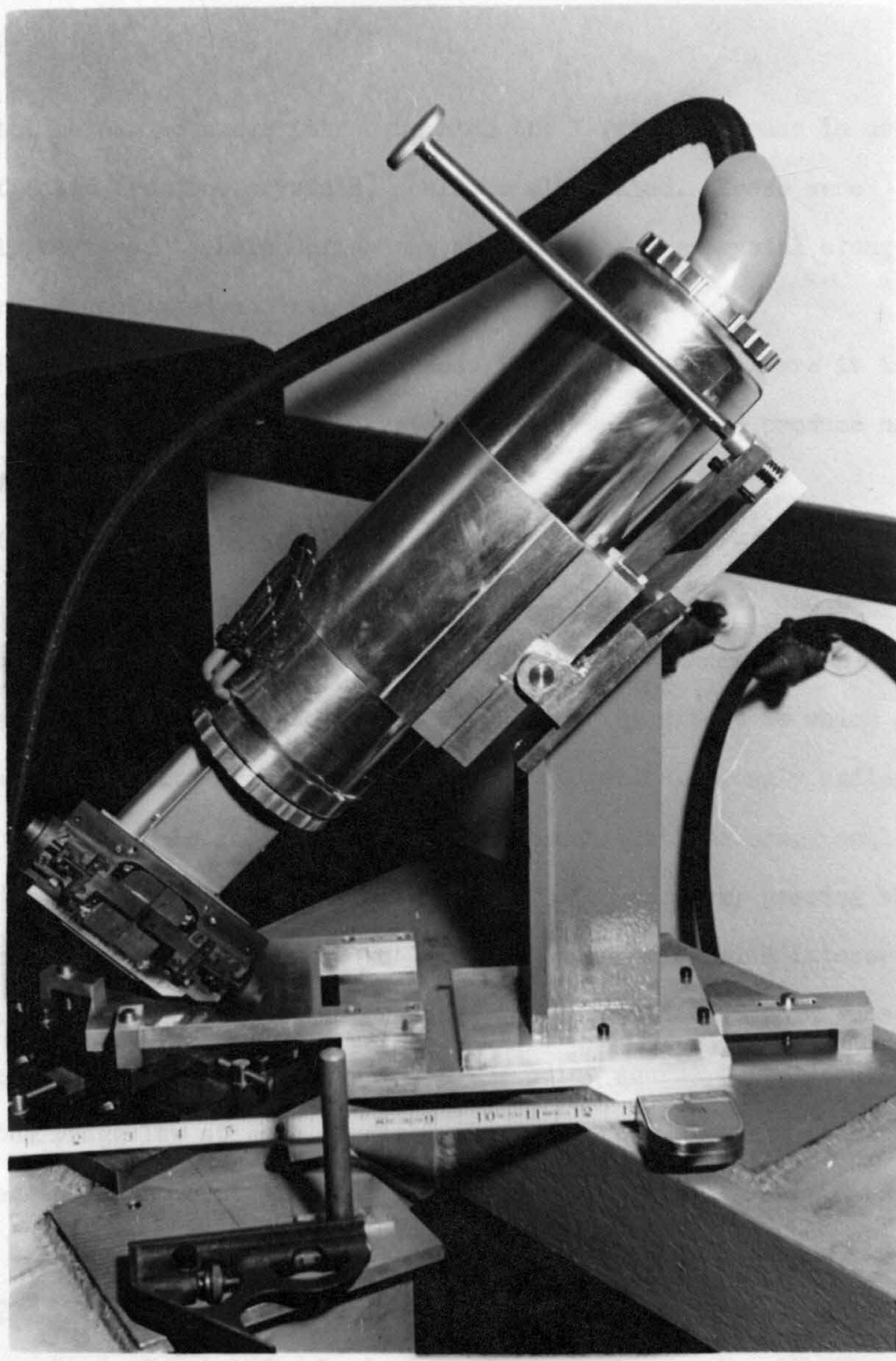


Fig. 21 New X-ray tube and mounting.

the crystal holder openings (through which the X-rays must pass in order to be reflected from the crystals) could be eliminated. These were originally designed to help define the curvature of the crystal along its otherwise unclamped central portion.

Point (1) is adequately discussed in reference (2) where it is shown that such a change in the crystal laminae used should produce nearly a fivefold gain in intensity.

The gain in intensity which might be obtained by (2), i.e., "roughing up" the surfaces of the present (quartz) crystals, can be estimated as follows: The solid angle which the monochromator can accept (and pass) from a point source is limited (1) by the extent to which an X-ray beam may deviate from the Bragg angle but yet be strongly reflected by the quartz crystals and (2) by the requirement that the Bragg angle be satisfied to this same extent at both crystals for each ray passing through the monochromator. It can be shown<sup>(2)</sup> that those rays which intersect the plane midway between the two crystals in a certain hyperbola whose eccentricity depends on the position of the point source quite accurately satisfy the Bragg law at each crystal. In particular, let the point source considered be at the central point of the useable target strip, in which case the hyperbola degenerates into a pair of orthogonal lines as shown in Fig. 22. Rays (from such a source) that strike the first crystal about 3 mm above the horizontal focal circle have a grazing angle with the crystal planes that is approximately 2" less than the corresponding grazing angle for rays in the plane of this focal circle. Since 1" is the maximum amount by which a ray can deviate from the Bragg law and still be strongly reflected, it is thus apparent that the crystal window for the point source

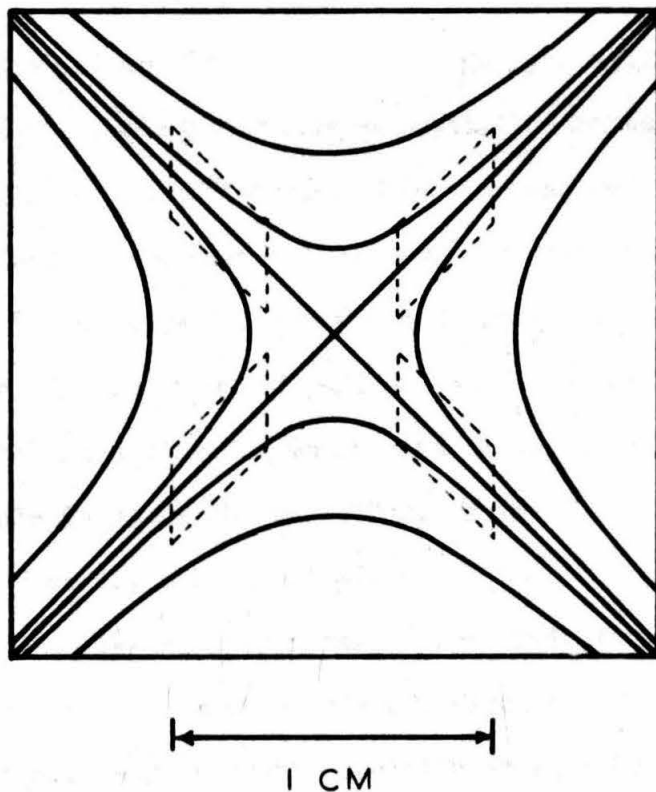


Fig. 22 Crosssection of the main X-ray beam in the region between the two crystals. The meaning and use of the hyperbolae and parallelograms shown are explained in the text.

under consideration consists of a strip along each of the intersecting lines mentioned above, each strip having a 3 mm "vertical width". For a given wavelength, there are thus four regions (one in each quadrant), each with an area of 9 sq. mm, in which a ray can intersect the plane shown in Fig. 22 and still be strongly reflected from both crystals. If, now, the surfaces of the crystals were slightly roughened so that the normals to the Bragg planes of some crystallites in the surface differed from the normals to the undisturbed planes by angles up to  $\delta$ , a gain in the X-ray intensity passed by the crystals would result. However, the magnitude of  $\delta$  is limited because of the resolution requirements that have been imposed. The width of the present focal spot (using highly polished crystal faces) is 0.2 mm and its distance from the plane between the two crystals is about 800 mm. Thus, if the focal width is not to be appreciably increased, one cannot allow  $\delta$  to be larger than about  $5 \times 10^{-5}$  radians. Taking this as the upper limit for  $\delta$ , the area of each of the four regions mentioned above becomes about 1000 sq. mm which is the full area of any quadrant. A similar result holds for the cases in which the point source considered is located elsewhere on the useable target strip. Allowing a factor of two to make up for overlapping of the regions and inability to fully expand regions at the edge of the crystals, and a similar factor to take account of the fact that some of the rays striking the perfect face of a curved crystal at a non-Bragg angle may penetrate the crystal and eventually meet the Bragg requirement, one could still expect a twenty-five fold gain in intensity as a result of the roughening process. The assumption that absorption in the crystallites is small compared to extinction (i.e., reflection of the radiation by the

Bragg law) has been implicitly made, but is not believed to affect the results appreciably. The real challenge seems to be that of finding a method for roughening the crystals by just the right amount so that full advantage can be taken of the increased intensity without spoiling the resolution.

The area of the webs is such that their removal would increase the intensity in the main monochromatic beam by about 20%.

#### Miscellaneous Improvements

Adjustable lead slit jaws have been mounted immediately in front of the window of the X-ray tube (see Fig. 21) so that the "length" of the point focus can be easily and continuously adjusted.

The nearly vertical column leading from the second crystal to the point focus has been constructed so that samples may be conveniently introduced at any one of four distances from the focal plane. As mentioned in Part I, the distance between any two of these positions is accurately known so that effective sample-to-film distance may be found experimentally. Another desirable feature of fixed sample positions is the ease it affords for making efficient use of the sample. The cross-section of the X-ray beam at each of the four sample positions can be easily found by exposing a film there, so that sample holders (a set for each position) can be made which allow only this cross-section to be covered by the sample. This efficient use of the sample is particularly important for work with bacteriophage where it is very difficult to prepare large samples.

The retainer which holds the detecting film in the focal plane has been carefully machined so that it can be removed for the process of changing films and subsequently replaced with exactly the same orientation.

In conjunction with the instrument for correcting for film shrinkage (see below), this provides a means for knowing quite accurately the orientation, with respect to the focal spot, of the diffraction pattern recorded on a given film. This feature is particularly important when small changes in size such as those sought in Part III are to be measured.

A device for correcting for film shrinkage has been constructed and is shown in Fig. 23. Its operation is as follows: A piece of (circular) film is placed in the holder provided, and oriented by means of a punch mark in the film. A carefully made disk (not shown in the photograph) keeps the film fixed in its holder. With the rectangular brass spacing block in position (as in Fig. 23), the film holder is pressed to the left until contact is made (1) between the holder and the spacer and (2) between the spacer and the end of the recess (which holds both the spacer and the film holder). The film is then exposed to visible light in a small region about 0.005 inches in diameter, this "spot" being about  $\frac{7}{16}$  inches from the center of the film. The source of illumination is a pen-type flashlight bulb, and the collimation necessary to give such a small well defined "spot" is accomplished by the use of two pin holes, each with a diameter of about 0.0045 inches, separated by about  $\frac{1}{2}$  inch. The box-like lower part of the apparatus houses the light source and a dry cell battery. After making the exposure with the spacer in place, this spacer is removed and the film holder is again pressed to the left, this time until it makes contact with the end of the recess. When in this position another spot exposure is made, the distance between the spots being accurately determined by the depth of the spacer (about  $1\frac{1}{8}$  inches). These spots do not interfere with the X-ray diffraction pattern

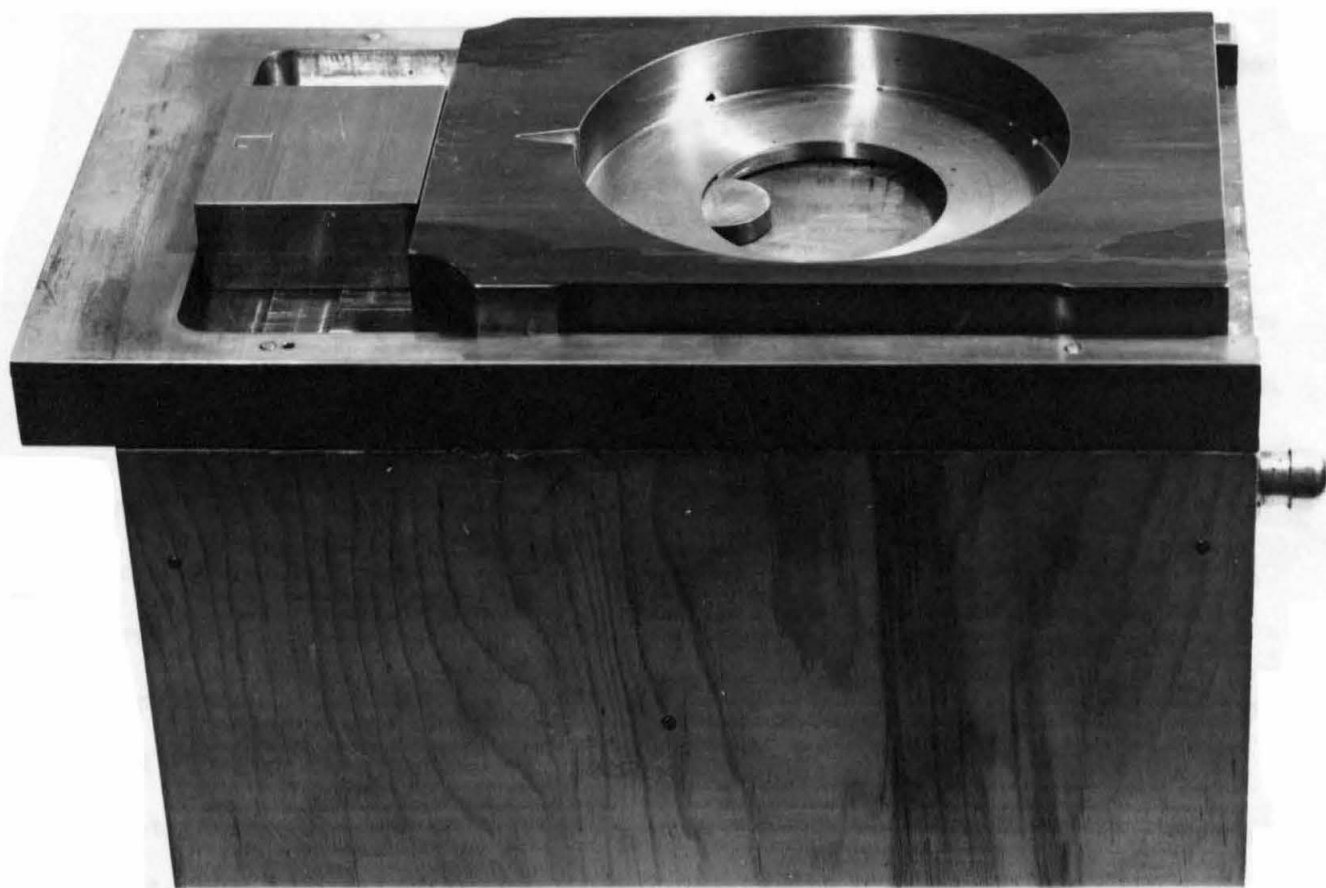


Fig. 23 A device for correcting for film shrinkage.

subsequently obtained. Care was taken to insure that contact between (1) spacer and holder, (2) spacer and recess, and (3) holder and recess occurs along the same line in the direction of film holder travel.

As well as providing a means for detecting film shrinkage, these spots also provide convenient indices for use in aligning the film (after its exposure to X rays) in the microphotometer.

#### Proposals for Further Applications

As has been intimated earlier, it is the author's belief that the point focusing monochromator will be most useful when used in conjunction with the electron microscope. The ability of the monochromator to use wet samples makes the whole field of phenomena connected with particle swelling more amenable to study than has previously been the case. Here the most fruitful procedure appears to be that followed in the investigations described in Part V: (1) the shape is found using the electron microscope, and (2) the shape is assumed to be only slightly changed in swelling so that (3) the amount of swelling can be found by comparison of the theoretically obtained intensity pattern (which, by assuming the shape to be known, depends on only a single length parameter) with that obtained experimentally. Interesting applications along these lines might be made, for example, in connection with the swelling properties of certain clays which are of importance because of their connection with underground oil reserves. A similar application would be to the study of particle size in certain Portland cements.

Other applications of a very fundamental nature in which small changes in particle size are measured seem particularly attractive subjects for study with this instrument. A suitable technique for performing such

measurements was developed in Part III where it was made clear that high precision in measuring a particle parameter demands equal particles similarly oriented. This prerequisite is believed met by certain biological particles such as the nearly spherical bacteriophage. In this connection a most interesting problem for investigation with the point focusing monochromator has been suggested by Dr. J. Weigle of the Biology Department of this institute. This is the study of these spherical bacteriophage to see whether the mean diameters of these macromolecular aggregates are changed when they are inactivated with antibodies. That such a change occurs is suspected by some biologists who believe the antibodies actually form a thin "coating" around the individual bacteriophage particles.

REFERENCES

1. J. W. M. DuMond, R.S.I. (1950) 21, 188
2. Leon Shenfil, Thesis, California Institute of Technology (1952)
3. J. W. M. DuMond and H. A. Kirkpatrick, R.S.I. (1930) 1, 90  
J. Johansson, Zeitschr. f. Phys. (1933) 82, 507
4. C. G. Shull and L. C. Roess, J. Appl. Phys. (1947) 18, 295 and 309
5. K. L. Yudowitch, J. Appl. Phys. (1951) 22, 214
6. C. H. Gerould, J. Appl. Phys. (1950) 21, 183
7. M. S. Gingrich and B. E. Warren, Phys. Rev. (1934) 46, 248
8. A. E. Rodriguez, Proc. Roy. Soc. A, (1949) 196, 73
9. G. Fournet, Acta Crystall. (1951) 4, 293
10. R. A. Pasternak and R. B. Corey, A report submitted January 11, 1952, to the Chairman of the Division of Chemistry (Calif. Inst. of Tech.) entitled "The Structure of Collagen"
11. R. S. Bear and O. E. A. Bolduan, Acta Cryst. (1950) 3, 236  
J. Appl. Phys. (1951) 22, 191
12. O. E. A. Bolduan and R. S. Bear, J. Polymer Sci. (1950) 5, 159  
J. Polymer Sci. (1951) 6, 271
13. A. Guinier, Ann. de Physique (1939) 12, 161
14. F. W. Putnam, Science (1950) 111, 481